

PFC/JA-81-4

IN SEARCH OF OPTIMIZED BUNDLE DIVERTORS

T.F. Yang, R. Potok, A. Wan, D. Blackfield

M.I.T. Plasma Fusion Center

J. Fisher

C.S. Draper Laboratory, Inc.

October 1981

By acceptance of this article, the publisher and/or recipient acknowledges the U.S. Government's right to retain a nonexclusive, royalty-free license in and to any copyright covering this paper.

# IN SEARCH OF OPTIMIZED BUNDLE DIVERTORS

T. F. Yang, R. Potok, A. Wan, D. Blackfield, (MIT)

J. Fisher, (Draper Lab)

PFC/JA-81-4

## Abstract

The perturbation due to the introduction of a bundle divertor into a tokamak system may induce ergodicity of the magnetic flux surfaces, enhance the diffusion loss of the thermal particles, and enhance the loss of energetic particles. It is shown here that these confinement characteristics can be optimized by carefully shaping the divertor coil configurations which meet the constraints for reactors. The toroidal vacuum field ripple and divertor current are minimized for various configurations to produce the same size of plasma. The magnetic flux surfaces are then calculated by combining the vacuum toroidal field with the axisymmetric MHD equilibrium flux surfaces. Most of these surfaces exhibit magnetic island structures, but are not ergodic. A large number of test particles are launched on a given flux surface with a pitch angle and energy distribution of an isotropic Maxwellian. The particle orbits are followed by using guiding center equations accurate to second order in  $\mu$ . Collisional effects are included through energy scattering, pitch angle scattering, and drag terms dependent on the background density and temperature. The energy containment of alpha and beam particles and thermal conductivity for both divertor and non-divertor cases are calculated and compared.

## 1. Introduction

Since the invention of the bundle divertor and the successful experiments on DITE [1,2], there has been interest in its application for reactors. The advantages and drawbacks have been discussed in many reactor feasibility studies [3,4,5,6]. The detailed confinement characteristics of a perturbed toroidal plasma in a tokamak with a bundle divertor have not been fully understood. Neither has an optimum divertor system been obtained which will meet the constraints of a power producing reactor.

The principle advantage of a bundle divertor is in its replaceability and potential for external particle and thermal power handling system. Because it is a local appendage, a specific design is possible such that the divertor can be decoupled from the remainder of the tokamak system. However, the axisymmetric property will be destroyed by the bundle divertor. The perturbation on the toroidal magnetic field, called the field ripple, may cause ergodicity in the magnetic flux surfaces. The banana orbiting particles may drift out due to the scattering by the ripple at the banana tip [7]. The containment of alpha particles and beam is a serious concern; thus, the ripple should be kept as small as possible. The bundle divertor creates a separatrix with its strong toroidal field; thus, the current required in the divertor coil is very large. The restraining of the large magnetic forces and torques is a difficult task. The need for keeping low ripple for confinement places a premium on reducing the size of the divertor coils. This, in turn, places a premium on reducing the thickness of neutron shielding space. The combined effect results in a very high current density and insufficient shielding. The high current density and magnetic stress make the use of superconductors difficult, and power consumption would be extremely high if a normal conductor were used to make the bundle divertor feasible for reactors.

In the next sections we see that the effect of the bundle divertor on the particle and energy confinements can be minimized by carefully shaping the divertor coil configuration so it will also meet the engineering constraints.

The most difficult engineering constraints are the current density in the conductor and shielding requirement. From practical experience 3 to 4 kA/cm<sup>2</sup> of current density is considered to be acceptable for both normal conductor and superconductor. The neutron shielding design study has shown that for a composite shielding material of tungsten and borated water of 60cm thickness, the life time can be from 1 to 100 MW-yr/m<sup>2</sup> for insulation materials tested in the dose limit of 10<sup>7</sup> to 10<sup>9</sup> Grays [8]. Therefore, the current density of 3.5 kA/cm<sup>2</sup> and shielding space of 60 cm are used as the maximum and minimum constraints throughout this paper.

In general the ripple is a good indication of whether a specific configuration is acceptable. It is found here that the ripple can be drastically reduced by carefully shaping and arranging the coils. The zero ripple point

can be placed near the center of the torus. Positive ripple can be produced in the inner side of the plasma torus where its effect is less important. Many configurations are compared under the same constraints. It is found that a staged T-shaped divertor configuration will give the least ripple, the best confinement, the least current, and smallest physical size. Therefore, it is considered to be the best configuration and is named a cascade bundle divertor. The detailed confinement characteristics of such a divertor are studied and discussed in Section 3. The engineering implications are discussed in Section 4. Specifically the whole divertor assembly is very compact and can be installed and removed as a plug-in unit. The coil can be superconducting so that the power loss is negligible.

To study the confinement the computation methods are as follows: The MHD equilibrium flux surfaces are obtained for a typical reactor plasma such as INTOR [9]. The flux surfaces are retraced by superimposing the axisymmetric equilibrium surfaces with the divertor coils. Prominent magnetic island structures were observed for the cascade divertor. The thermal particles, alpha particles, and beam particles are launched on the flux surfaces. Their orbits are tracked by using the guiding center equation to the second order of the magnetic moment  $\mu$ . The thermal conductivity  $\chi$  and power containment of alpha and beam particles are computed for both divertor and no-divertor cases.

## 2. Magnetics

The first DITE type bundle divertor consists of two solenoids of constant radius [1]. The ripple on the axis of the plasma is as high as 3%. The energetic particles will walk out due to the scattering at the banana tip [7] or drift out if trapped inside the ripple. The ripple will also enhance the diffusion loss [10]. All these losses will be proportional to the number of particles trapped in the ripple, which is in turn proportional to  $\sqrt{\epsilon}$ , where  $\epsilon$  is the ripple amplitude. Therefore, the first task is to reduce the ripple. Another serious direct loss is due to the ergodicity of the magnetic surfaces. The second task is thus to make certain that the magnetic surfaces will not become ergodic when the bundle divertor is added to the system. The third task is to check the confinement of the plasma, energetic alphas and beam particles.

Many coil configurations have been proposed to reduce the ripple or to reduce the current density. Ten different configurations have been studied and are illustrated by picture (a) in Figs. 1 through 10. Picture (b) in these figures are the toroidal flux configurations on the equatorial plane. There is no auxiliary field correction coil. All these divertors can be constructed as a single unit and will be called simple divertors. Further improvement with the use of many auxiliary coils is not the subject of this paper. Figure 1 shows the straight solenoidal coils as of original DITE design. The radius of the solenoids in Fig. 2 is expanding; thus, the current density can

be reduced by distributing the turns over larger area [5]. Figure 3 is the "X" shaped solenoidal coils, which was proposed by Dory to reduce the ripple [6]. As in a tokamak, the magnetic field drops to zero at large distance from the "X" coils. Shown in figure 4 are the rectangular shaped coils. Figure 5 shows the coils which are bent into "T" shape to reduce both ripple and current [10]. The horizontal elements will increase the field intensity locally; thus, the current and ripple can be both reduced. Figure 6 is a double "T" shaped divertor. Figures 7 and 8 show the effect of different arrangements of "T" coils.

Let us first compare the ripple produced on the axis from these coil configurations. The results of these configurations are summarized in Table 1. Configurations 1 and 2 are large size coils. The divertor coils of configurations 3 through 9 are all of same size such that they all are removable as a single unit. Toroidal ripple is defined as

$$\epsilon = \frac{B_{\text{peak}} - B_0}{|B_{\text{peak}} + B_0|} \quad (1)$$

calculated along a field line originated from the centerline of the divertor where  $B_0$  is the field at the center line of the divertor. On the inner side of the plasma the field intensity is actually increased for some configurations. Therefore,  $\epsilon$  can be positive or negative. The ripple on axis for all these configurations is plotted in Fig. 9. The simple straight solenoids have the worst ripple. The "X" shaped and two reversed "T" coils are in the middle. The "T" shaped arrangements give the lowest ripple. The ripples for the "T" shaped coils are even negative at the radii less than 4.8 m. The ripples for the multiple "T" coils for various sizes all fall in the shaded region.

The current, current density, and ripple on axis,  $R = 5.4$  m, are listed in Table 1. The current densities are calculated for the largest coil having a cross-section of  $50 \text{ cm} \times 50 \text{ cm}$ . For all the configurations other than "T" shaped coils, the current requirements are very large and the current densities are not practical for engineering consideration. To reduce current density the coil radius or width has to be increased. This makes the coil maintenance difficult.

By examining the flux configurations for the "X" and reversed "T" coils, it is seen that the fluxes are very tight at the divertor region. Varying the openings of the outer legs of the "T" gives very little improvement. The magnetic field intensity in this region is higher than 10 T. Therefore, further expansion by reducing the field would require huge current. The double "T" shaped coils give the best expansion, lowest ripple, and smallest current density. Therefore, the "X" and reversed "T" coil configurations can be eliminated from a practical standpoint. The ergodicity of the magnetic surfaces for solenoidal coils with constant radius, expanding radius, and "T" shaped coils were studied and are now discussed.

To compute the flux surfaces the axisymmetric MHD equilibrium surfaces are superimposed with the

perturbed toroidal field. The poloidal flux surfaces are computed by using the Pest code [13] and are shown in Fig. 10. The plasma parameters are  $R_o = 5.4$  m,  $a = 1.6$  m,  $\beta = 6\%$ ,  $q = 2.8$ ,  $I_p = 7.8$  MA and  $B_o = 5.3$  T, which are typical of a power reactor. This was chosen for the purpose of illustrating the engineering feasibility in Section 4. Some care is needed to select the poloidal flux configuration for a high  $\beta$  noncircular plasma. For a noncircular high  $\beta$  plasma the flux surfaces are closer together in the area beyond the magnetic axis. The poloidal separatrix is very close to the plasma surface even if it is defined by a limiter or toroidal separatrix. As shown in Fig. 10, the poloidal separatrix is more than 20 cm away, larger than the scrape-off layer, otherwise the poloidal divertor would be competing with the limiter or bundle divertor. On the inner side of the plasma the flux surfaces are less dense and the wall has to be at least 30 cm away; otherwise, the inner wall will become the effective limiter. These are common problems for both bundle divertor and mechanical limiter methods.

The flux surfaces computed at  $\phi = 0^\circ$  and  $180^\circ$  for the configurations 1, 2, 5, 6 and multiple T-coils are shown in Figs. 11, 12, 13, 14 and 15. The fluxes for straight solenoids and single T coils are ergodic. The flux surfaces for solenoids with expanding radius, double T and triple T are nonergodic. On the  $\phi = 0^\circ$  plane, mid-plane of the divertor, the toroidal field is weak; thus, the shear is large. The field lines are moving faster in the poloidal direction; thus, the line density is reduced. Four magnetic surfaces are computed and displaced in Fig. 15 for stacked three T coils. The surface close to the center happens to be at  $q = 1$ ; therefore, no surface is traced even after a hundred turns along the torus have been followed. All the surfaces exhibit island structures. The islands on the surface next to the boundary are large. Therefore, further improvement is needed to reduce the island size.

### 3. Confinement Characteristics

In the previous section we have determined that the cascade "T" bundle divertor is the optimum configuration. It is not detrimental to the gross confinement since the flux surfaces are nonergodic. In this section we would like to test the microscopic confinement characteristics by following the guiding center orbit of the test particles and study the effect of the ripple on particle diffusion.

Let us first examine the ripple diffusion coefficients. The enhancement of diffusion coefficients due to the toroidal ripple has been discussed by many authors [12,14,15]. The toroidal ripple has mode number  $N$  (equal to the number of divertors) and the ripple can be represented by sinusoidal function of  $\phi$ . The divertor ripple is 100% at the separatrix. However, the ripple is localized and its magnitude decreases exponentially. Only one divertor is being considered presently. The effect on the diffusion coefficients due to these two types of divertors

is different. To illustrate this difference the ripple plateau particle diffusion coefficient and thermal conductivity are rederived.

The toroidal field due to the presence of toroidal ripple  $\delta_t$  and divertor ripple  $\delta_d$  can be written as

$$B = B_o(\psi) \left( 1 + 2\epsilon \sin \frac{2\theta}{2} + \delta_t \sin N\phi + \delta_d \exp \frac{-(\phi - \phi_o - \pi/N)^2}{2\alpha} \right). \quad (2)$$

For trapped particles  $\mu B_o \simeq mv^2/2$  and in ordinary  $r, \theta, \phi$  toroidal coordinates, the radial ripple drift is

$$(v_r)_r = \frac{\rho_\theta v}{2R} N \delta_t \left[ \cos(N\phi) - \frac{(q\theta - \pi/N)}{\alpha} \frac{\delta_d}{\delta_t} \exp \frac{-(q\theta - \pi/N)^2}{2\alpha} \right] \quad (3)$$

with  $\rho_\theta = v(mc/eB_o)^{-1}$  and for  $\delta_t > 0$ . Following the procedure given in Ref. 12 the ripple diffusion coefficient for  $\delta_t > 0$  can be written as

$$D = \left( \frac{\pi}{2} \right)^{1/2} N^2 \langle \delta_t^2 \rangle \rho_\theta^2 \frac{v_{th}}{R} \frac{B}{b_\phi} \left[ 1 + \frac{1}{2\pi Nq} \langle \delta_d^2 \rangle / \langle \delta_t^2 \rangle \right] \quad (4)$$

for nearly circular flux surfaces, where  $\langle \delta^2 \rangle$  is the averaged value over the flux surface. The thermal conductivity can be written as

$$K = \frac{15}{2} \left( \frac{\pi}{2} \right)^{1/2} n N^2 \langle \delta_t^2 \rangle \rho_\theta^2 \frac{v_{th}}{R} \frac{B}{b_\phi} \left[ 1 + \frac{1}{2\pi N^2 q} \langle \delta_d^2 \rangle / \langle \delta_t^2 \rangle \right]. \quad (5)$$

At the boundary  $\frac{1}{2\pi N^2 q} \langle \delta_d^2 \rangle / \langle \delta_t^2 \rangle$  is approximately 2. That is, the diffusion due to divertor ripple is enhanced by a factor of 2.

The thermal conductivity is also computed numerically using a Monte Carlo guiding center particle orbit code [16]. The guiding center equations, which are accurate to the second order, are

$$V_{\parallel}^2 = \frac{2}{m} (E - \langle \mu \rangle B_{GC}) + 0(\epsilon^2) \quad (6)$$

$$V_{\perp} = \frac{\epsilon}{B} \hat{b} \times \left[ \frac{\langle \mu \rangle}{m} \nabla B + V_{\parallel}^2 \hat{b} \cdot \nabla \hat{b} \right] + 0(\epsilon^2) \quad (7)$$

and

$$\frac{dV_{\parallel}}{dt} = -\frac{\langle \mu \rangle}{m} \hat{b} \cdot \nabla B + 0(\epsilon). \quad (8)$$

Particle conservation for these equations of motion is confirmed by the drift kinetic equation  $\underline{V} \cdot \nabla f = 0$  [12]. The particle pushing algorithm is now briefly described.

A two dimensional spline interpolation is used to compute B and its gradient from the MHD equilibrium flux configurations, and is superimposed by the field and gradient computed from divertor coil geometry. The guiding center is launched along its initial velocity direction, keeping toroidal and radial velocity constant. The energy conservation is incorporated in the pushing algorithm directly because guiding center equations conserve energy to at least two orders. As a particle approaches a reflection point, i.e., when  $|V_{\parallel}| < |V_{\perp}|$ , the predictor point of the pushing algorithm is found by following the local B field line to the next  $\phi$ -plane. This results in a more accurate average of the particle's motion between the two  $\phi$ -planes.

In computing the MHD equilibrium flux surfaces the toroidal field profile used is [13]

$$B_t = B_o R_o \left[ 1 - g_p \left( \frac{\psi - \psi_o}{\psi_L - \psi_o} \right)^\alpha \right], \quad (9)$$

and the pressure profile used is

$$P = P_o \left( \frac{\psi - \psi_o}{\psi_L - \psi_o} \right)^\beta, \quad (10)$$

where  $\psi_o$  and  $\psi_L$  are fluxes at the magnetic axis and limiter, respectively.  $P_o$  is the peak pressure and  $\alpha$ ,  $\beta$  and  $g_p$  are constants. To obtain temperature and density profiles we write

$$\begin{aligned} P &= n_o(\psi) T_o(\psi) \\ &= n_o T_o \left( \frac{\psi - \psi_o}{\psi_L - \psi_o} \right)^{\beta_n} \left( \frac{\psi - \psi_o}{\psi_L - \psi_o} \right)^{\beta_T} \end{aligned} \quad (11)$$

with  $\beta_n + \beta_T = \beta$ . To study the interaction of the alpha particle with background plasma we use the electron drag on alphas [16]

$$\frac{dU_\alpha}{dt} = \frac{q_\alpha^2 q_e^2 n_e m_e (\ln \Lambda) [1 - 2U_\alpha / 3k_B T_e]}{\left[ 1 + \frac{4}{3\sqrt{\pi}} \left( \frac{m_e U_\alpha}{m_\alpha k_B T_e} \right)^{3/2} \right] 2\pi \epsilon_o^2 m_\alpha \sqrt{2\pi m_e k_B T_e}} \quad (12)$$

with

$$\Lambda = \frac{12\pi(\epsilon_o k_B T_e / e^2)^{3/2}}{\sqrt{n_e}} \quad (13)$$

The ion-alpha pitch angle diffusion is calculated from [16]



$$\frac{\langle (\Delta v_{\perp})^2 \rangle}{\Delta t} = \frac{n_i Z_i^2 e^4 \ln \Lambda}{2\pi \epsilon_0^2 m_{\alpha}^2 v_{\alpha}} \left[ I\left(\frac{v_{\alpha}}{v_{thi}}\right) - G\left(\frac{v_{\alpha}}{v_{thi}}\right) \right] \quad (14)$$

where  $\phi(X) - G(X) \simeq 1$  for  $X \gg 1$ . The ion-alpha drag is [16]

$$\frac{\langle \Delta V_{\parallel} \rangle}{\Delta t} = \frac{-n_i Z_i^2 Z_{\alpha}^2 e^4 \ln \Lambda}{2\pi \epsilon_0^2 m_{\alpha}^2 v_{thi}^2} \left( 1 + \frac{m_{\alpha}}{m_i} \right) G\left(\frac{v_{\alpha}}{v_{thi}}\right) \quad (15)$$

where  $G(X) \simeq \frac{1}{2X^2}$  for  $X \gg 1$ .

After the particle has been pushed from one  $\phi$ -plane grid to another in time  $\Delta t$ , the energy given to the electron and DT ions is calculated from the equations

$$Q_e = -\Delta t \frac{dv_{\alpha}}{dt} \Big|_{\text{electron drag}} \quad (16)$$

$$Q_i = \Delta t U_{\alpha} / (.385 \tau_{ia}^{\text{scat}}) \quad (17)$$

$Q_e$  and  $Q_i$  are then subtracted from the particles kinetic energy, while keeping the velocity space direction fixed. The particle's value for  $\mu$  is recomputed. Typically several hundred test particles simulating a maxwellian distribution are launched and tracked for hundreds of milliseconds. The particles launched outside the ripple are well confined. The orbits of the particles launched inside the ripple are of particular interest. Some representative cases are now discussed.

Three 3.5 MeV alpha particle orbits are shown in Figs. 17, 18 and 19. The coordinate system for the guiding center orbit ( $x, y, z$ ) corresponds to the ordinary toroidal coordinate system ( $r, z, \phi$ ). From top to bottom on the left column are the  $Y$  coordinates of the particle, toroidal angle  $\phi$ , energy and poloidal flux as functions of time. The first and second pictures on the right column are the projections of the orbits on the midplane of the divertor and on the equatorial plane of the tokamak respectively. The third and fourth pictures are the  $\cos \xi = v_{\parallel}/v$  and  $X$  position of the guiding center as functions of time respectively. They are typically circulating particles, banana particles and drifting particles. The first two types of orbits show the periodic variation of  $x, y, \phi$ , phase angle  $\xi$  and flux  $\psi$ . The variation of  $\xi$  and  $\psi$  and the orbit show a blip when the particle passes through the midplane of the divertor. These are well behaved orbits. The third orbit is clearly drifting out of the plasma. The phase angle is oscillating much more rapidly for the trapped particle as compared to the banana and circulating particles. Collision and electron drag have very little effect on the  $\alpha$ -particle orbit in such a short time; therefore, the drifting particle will be lost.

Figures 21, 22, 23 and 24 show the typical orbits of 10 keV thermal particles. It is particularly interesting to note that the orbit in Fig. 20 is detrapped from the ripple after a short time by observing that  $\xi$ ,  $Y$ ,  $\phi$  changing from short period into long period oscillation. The particle shown in Fig. 21 will eventually drift toward the outside of the plasma. However, this particle will be detrapped due to collision as shown in Fig. 22. As can be seen from the variation of  $\phi$  it changes from trapped into banana, then into circulating. The detrapping effect due to collisions is further demonstrated by Fig. 23 where the trapped orbit becomes a banana orbit in a short time. From the limited number of particles analyzed the majority of the circulating and banana particles do not become trapped due to scattering whereas the effect is opposite for the trapped particles. The particle launched at the plasma edge escaped to the divertor as shown by Fig. 24. The results are not conclusive because only a limited number of test particles are sampled. Due to lengthy computational time involved, the diffusion coefficients study is still in progress.

The preliminary results indicate that the thermal conductivity and particle loss can be reduced by moving the divertor away from the plasma. One important finding is that the toroidal separatrix should be 5 cm away from the plasma boundary due to the finite width of magnetic islands on the surface. Otherwise, the particle loss and thermal conductivity would be very large. The computed thermal conductivity is  $k = 1.07 \pm 0.12$  by launching 180 particles on the flux surface in the middle of the plasma.

#### 4. Engineering Implications (Feasibility)

As is discussed in the introduction, the most attractive feature of a bundle divertor is its maintainability and the possibility for external cleaning. However, the high current density, large forces, and lack of shielding spaces make the bundle divertor engineering difficult. This section will examine the answer to these problems for the configurations studied. Let us specify the criteria for a feasible divertor. In order to keep the power consumption low the divertor coil has to be superconducting. The reasonable average current density for a stable superconducting coil at 10 T maximum field should be less than 5 k Amp/cm<sup>2</sup> [5]. A commercial Nb<sub>3</sub>Sn cable which can carry 3.5 k Amp/cm<sup>2</sup> is available. Therefore this value is chosen as the current density criterion. In order to protect the insulation material and the superconductor a 60 cm shield of Tungsten and borated water composite is chosen which will give a life time of 5 years [8]. The forces are not the worst problems. A 100 MN force can be properly handled [5]. However, it should be kept as low as possible. The force is reduced when the current and coil size are reduced and the divertor coils are situated in the weaker toroidal field region. The last criterion allows easy maintenance by means of a plug-in unit.

From Table 1 one will notice that the current densities for configurations 1 and 2 are quite reasonable. However the size is too large and it is blocked by TF coils. The force would be as large as 100 MN and the maintenance procedure is very difficult, although not impossible. The current density for configurations 3, 4 and 5 are much too high. The configurations 5, 6 and 7 are ruled out because of poor confinement or impracticality. The current density for configurations 8 and 9 is less than 3.5 k amp/cm<sup>2</sup>. The sizes are smaller than the space between the TF coils. The outward translational force is much smaller which is about 20 MN. There is 60 cm of shielding space in front of the coils facing the plasma. Therefore these configurations satisfy the engineering criteria as well as giving good confinement. The divertor coil height has been varied from 1.4 m to 2.2 m and the distances from the plasma have been varied from 1.0 m to 1.2 m. The flux surfaces for these cases are all nonergodic and ripple is reasonable. Therefore 2.2 m height is chosen to accommodate a 60 cm shielding space, and a hole of 50 cm for plasma exhaust. The current increases from 8.75 to 12.3 and 13.55 MA-T when the distance increases from 1.0 m to 1.1 m and 1.2 m. However, the current density can be kept constant by increasing the conductor cross-section proportionally. There is more room for shielding even if the conductor cross-section is increased due to larger current at large distance. This demonstrates that a range of designs can be obtained. The choice is a matter of trade-off. A detailed three dimensional neutronic study is currently in progress to determine the adequate shielding space.

The engineering concept of a cascade bundle divertor and a monolithic bundle divertor assembly are shown by Figs. 25 and 26. The divertor assembly is a single unit construction. The forces are transmitted to TF coils through the two horizontal bars and heat stations which are specially designed to minimize the heat leakage and disconnection time. The bars are keyed to the divertor casing and attached to the heat station by a cylindrical bearing. The divertor assembly can be freed and extracted simply by lifting up and dropping down the bars. In a separate study the divertor coil can be constructed from cryogenic normal coils (copper or aluminum) and cooled by helium gas at 20-40 K. The dominant power requirement is refrigeration, which is about 20 to 50 MW. The use of normal coil requires slightly higher power consumption but allows easier fabrication. Therefore, both superconducting coil and cryogenic normal coils are feasible.

## 5. Conclusion

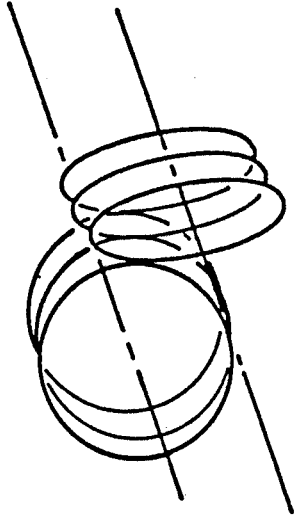
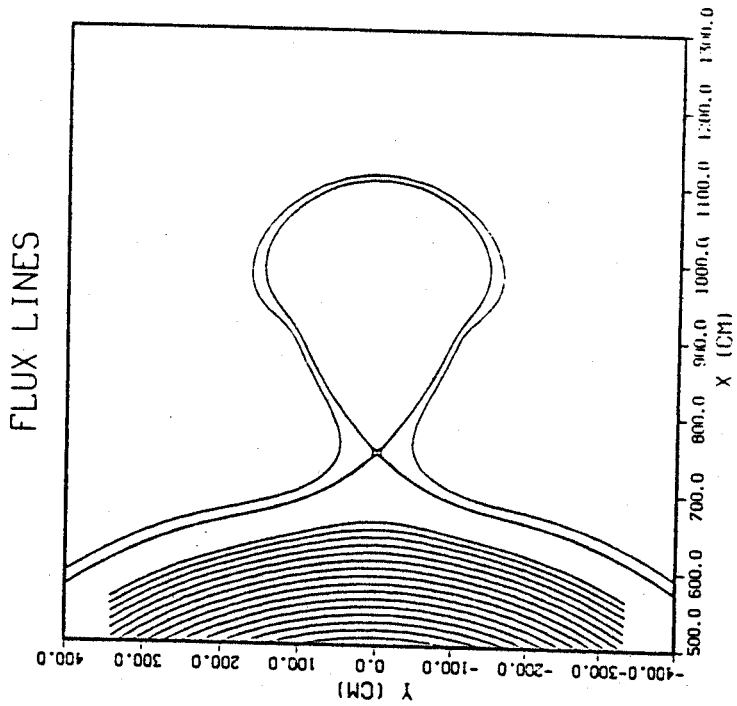
It has been shown in this paper that the gross particle confinement can be greatly improved by optimizing the bundle divertor confinement. A wide range of configurations exists which does not cause ergodicity on the flux surfaces in the plasma, although magnetic islands are created by the ripple. Therefore, there is no direct loss. The reduction of ripple on axis is about one order of magnitude. A very important finding is that the

equilibrium configuration has strong influence on the effectiveness of the divertor, especially for the high  $\beta$  where the poloidal separatrix has to be carefully located outside the scrape-off layer. It is also found that the cascade T-shaped divertor can be designed such that the key engineering constraints can be met.

The magnetic surface tracing and particle tracking are not exact because the field is a superimposition of the axisymmetric MHD equilibrium flux with the divertor field. Future investigations might use the results of a three dimensional equilibrium calculation. Also, further improvement in confinement can be done by using high order auxiliary coils. An extensive computational study is needed to determine the effect of the divertor by tracking particles escaping from the plasma edge. Lastly, the particle transport in the divertor and  $\beta$  and  $q$  dependences should be studied.

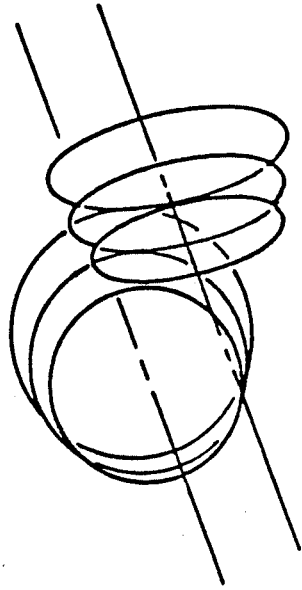
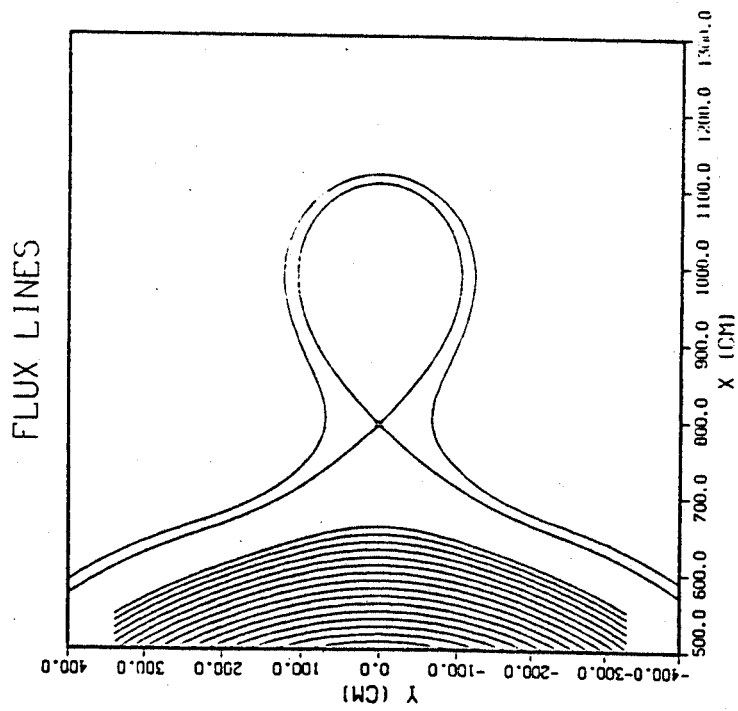
### References

- [1] Stott, P. E., Wilson, C. M., Gibson, A. "The Bundle Divertor - Part I; Magnetic Configuration", Nuclear Fusion, Vol. 17 #3, 481 (1977).
- [2] Stott, P. E., Wilson, C. M., Gibson, A. "The Bundle Divertor - Part II; Plasma Properties, "Nuclear Fusion 184, 475 (1978) and references cited.
- [3] Grawley, H. J., "The Practical Feasibility of a Bundle Divertor for a Tokamak Power Reactor", Proc. Ninth Symposium on Fusion Technology, Garmisch-Partenkirchen, W. Germany (1976).
- [4] Sanderson, A. D., Stott, P. E., "A Bundle Divertor for Fusion Reactor", CLM-P530, Culham Laboratory, Abingdon, Oxfordshire, England (1978).
- [5] Yang, T. F., et al, 8th Symposium, IEEE, San Francisco (1979).
- [6] Sheffield, John, Dory, R. A., "The Ripple Bundle Divertor for Tokamaks", ORNL-TM6220 (March, 1978) and US INTOR Report (1979).
- [7] Rome, J. A., Private Communication.
- [8] Cheng, E. T. C, Yang, T. F., "The Reflector-Shield Concept for Fusion Reactor Design", Trans. Am. Nucl. Soc. 34, 49 (1980).
- [9] Stacey, W., US INTOR Report, Phase I (1980).
- [10] Yang, T. F., US-Japan Workshop.
- [11] Furth, H., Ludescher, C., US INTOR Report (1979).
- [12] Boozer, Allen H., "Enhanced Transport in Tokamaks Due to Toroidal Ripple". P. F. 23, 2283 (1980).
- [13] Pest Code, PPPL.
- [14] Tsang, T., Frieman, E. A., "Toroidal Plasma Rotation in Axisymmetric and Slightly Nonaxisymmetric Systems", Phys. Fluids 19, 747 (1976).
- [15] Potok, R. E., Lidsky, L. M., Politzer, P. A., PhD Dessertation, PFC/RR-80-15 (1980).



Perspective view of  
divertor coils

Fig. 1: Bundle divertor of DITE type. The divertor coils are solenoids of constant radius. The coils are large and blocked by TF coils.



Perspective view of  
divertor coils

Fig. 2: Improved bundle divertor. The divertor coils are conical section whose radii are expanding. The current required is less, but coil is still large.

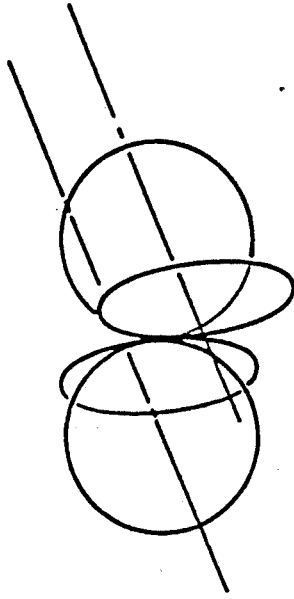
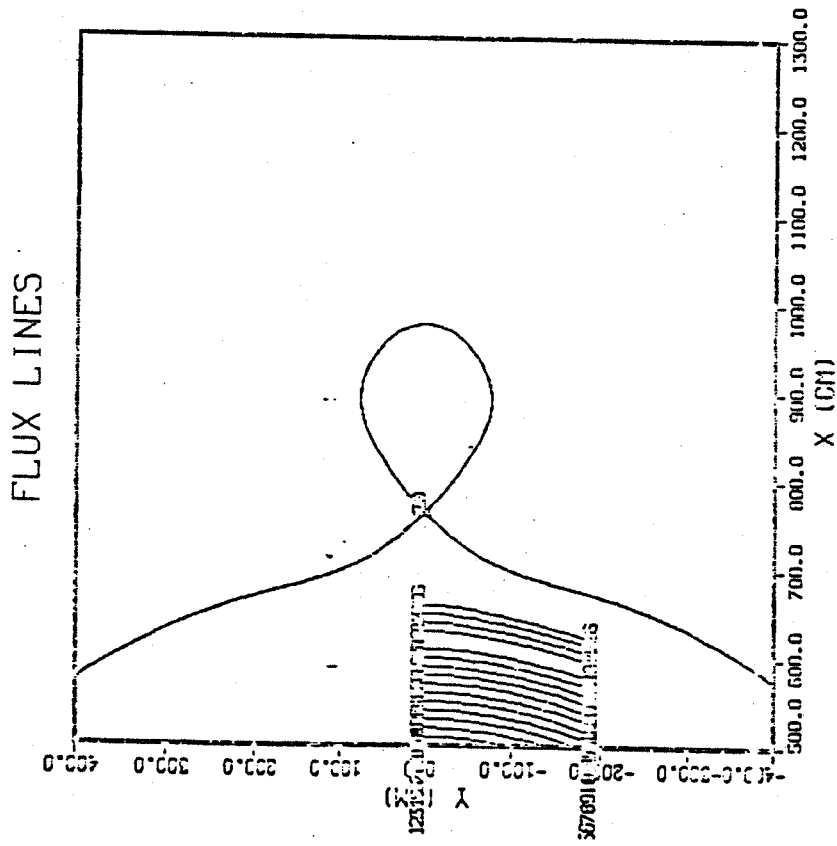


Fig. 3: "X" type bundle divertor. The divertor itself is like a small toroidal system; thus, the ripple is reduced.



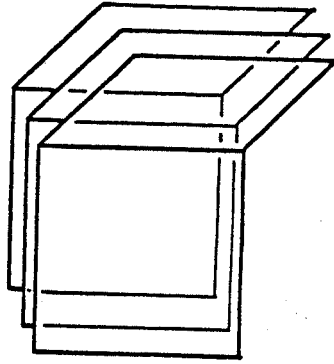
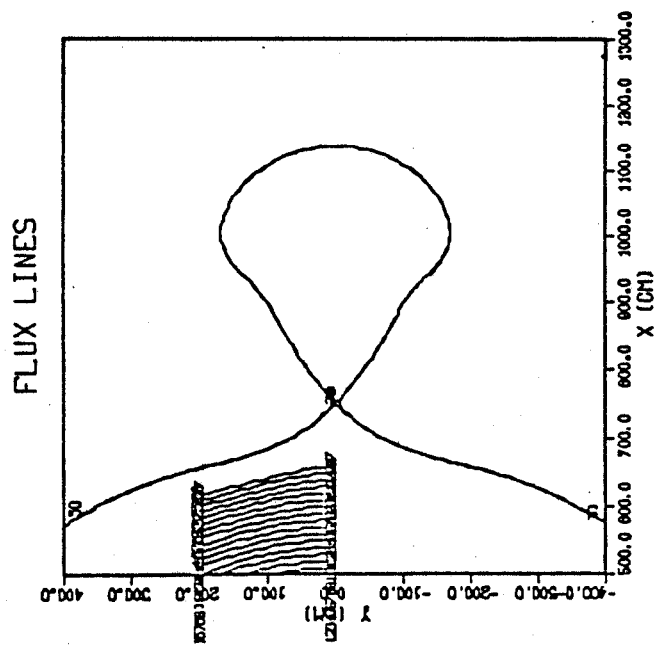


Fig. 4: Rectangular shaped divertor

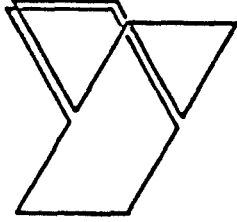
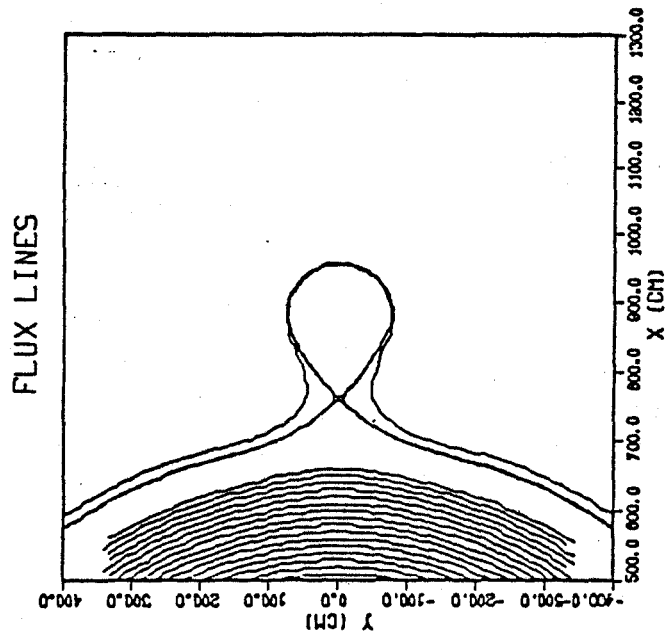


Fig. 5: "T" shaped bundle divertor. The divertor size can be constrained within space between TF coils so that the removal for maintenance is much simpler.

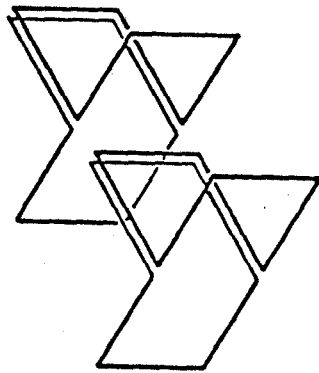
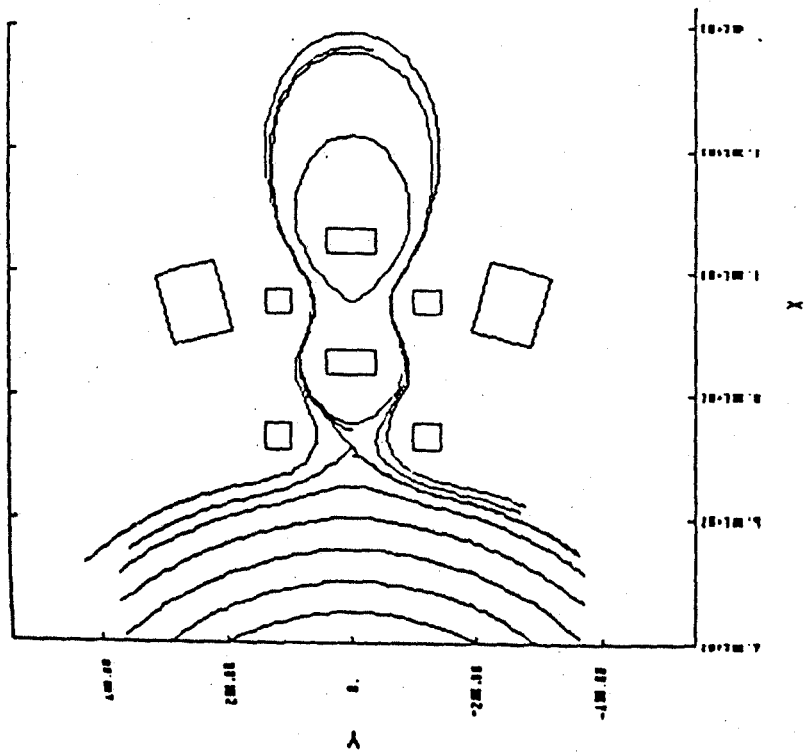


Fig. 6: Double "T" shaped divertor

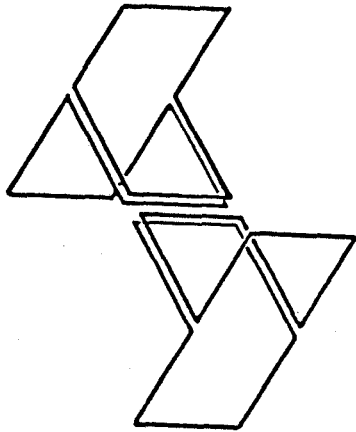
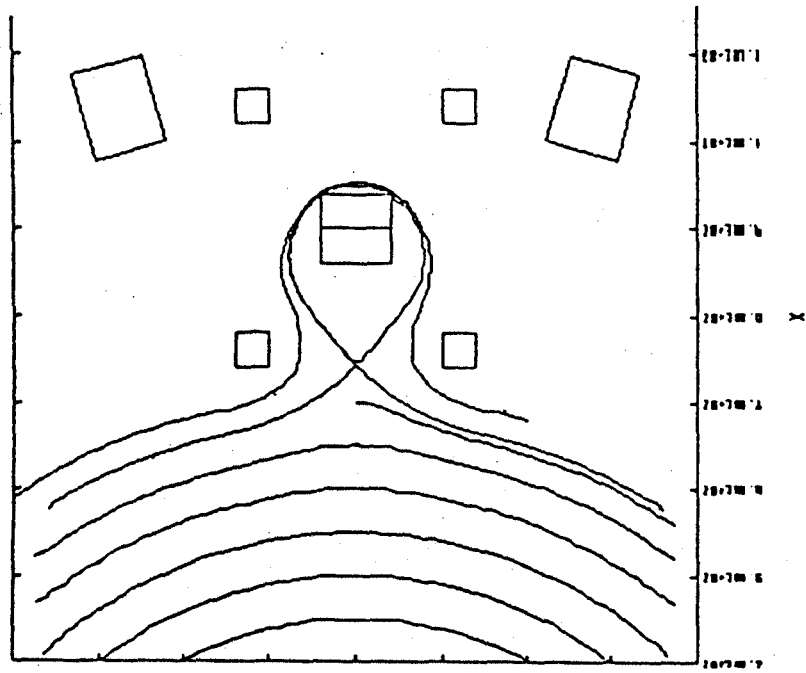


Fig. 7: Double "T" with reversed arrangement

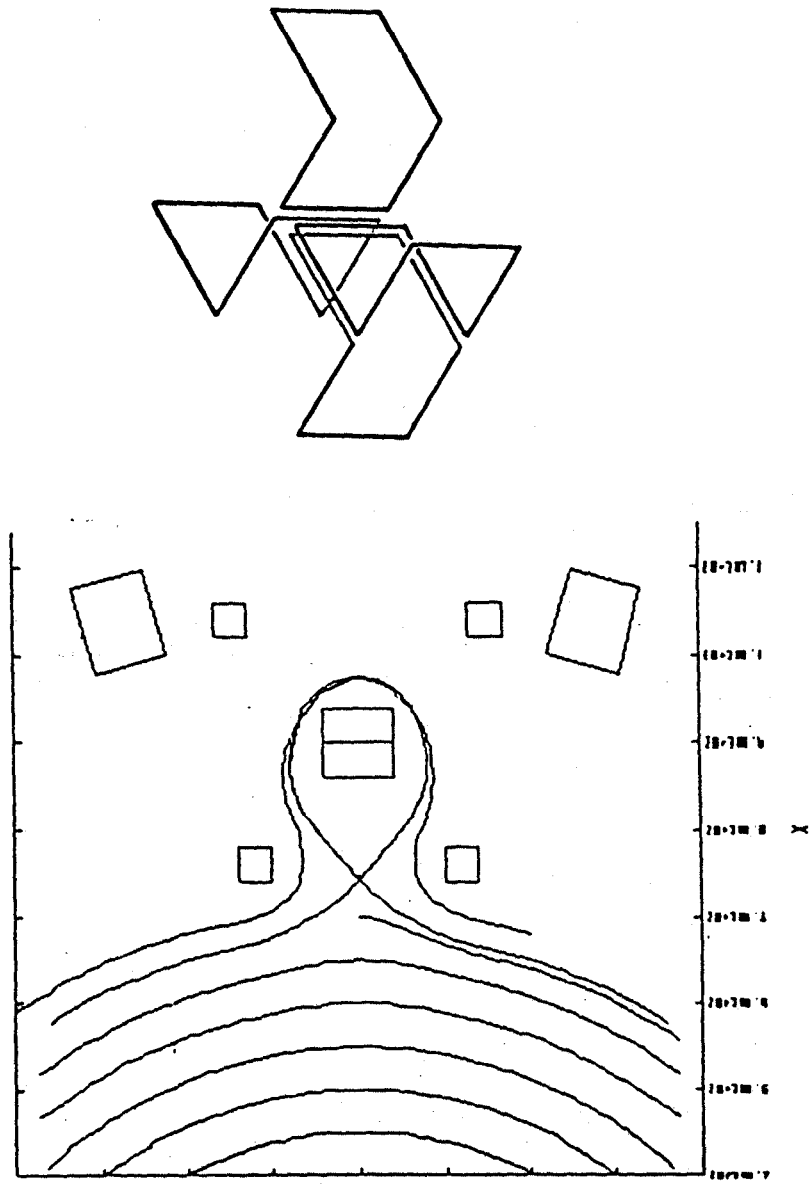


Fig. 8: "T" and "L" shaped divertor

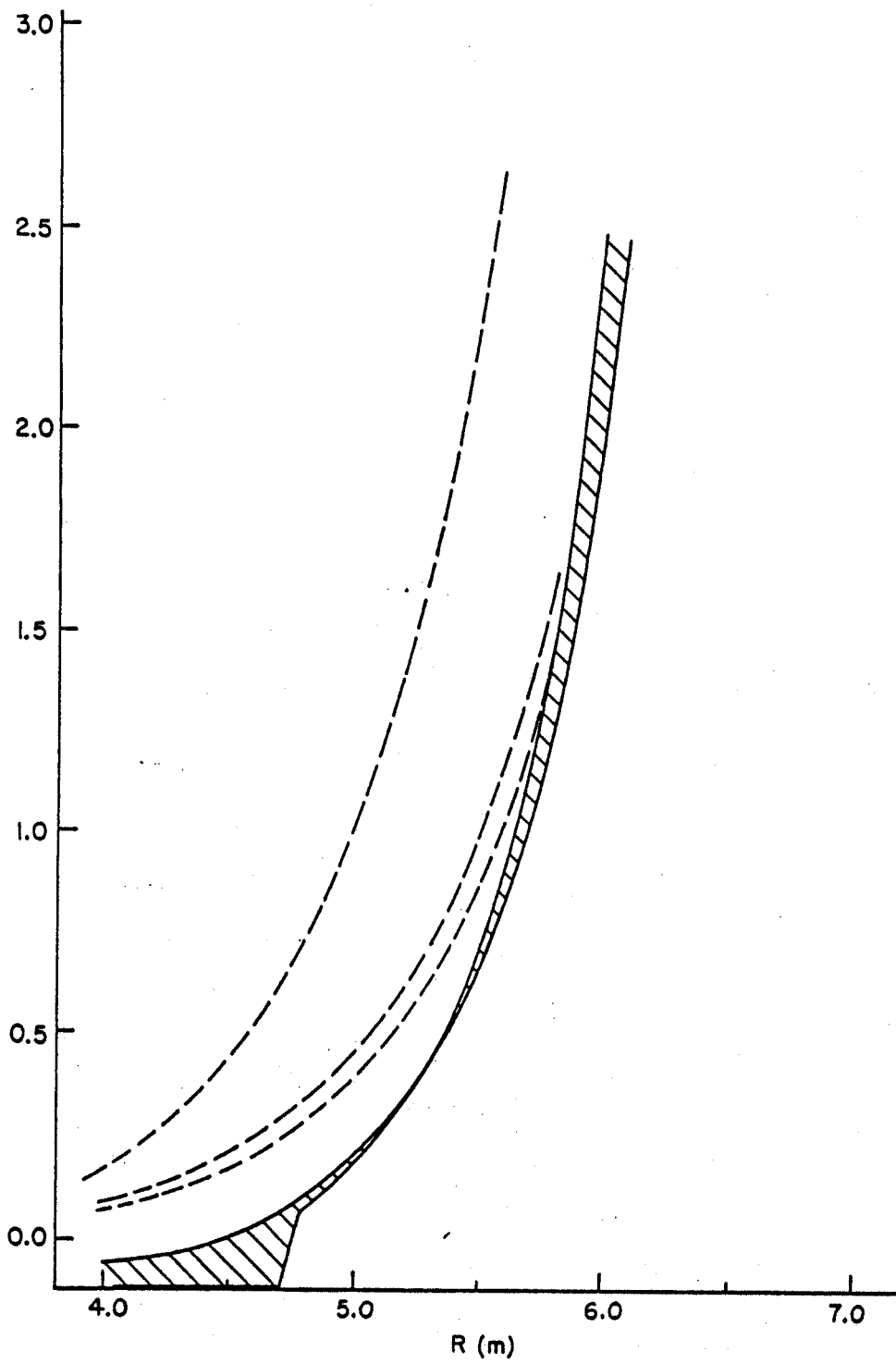


Fig. 9: Divertor ripple on axis for the configurations studied. The ripple for single "T" and cascade are the lowest. They all fall within the shaded region.

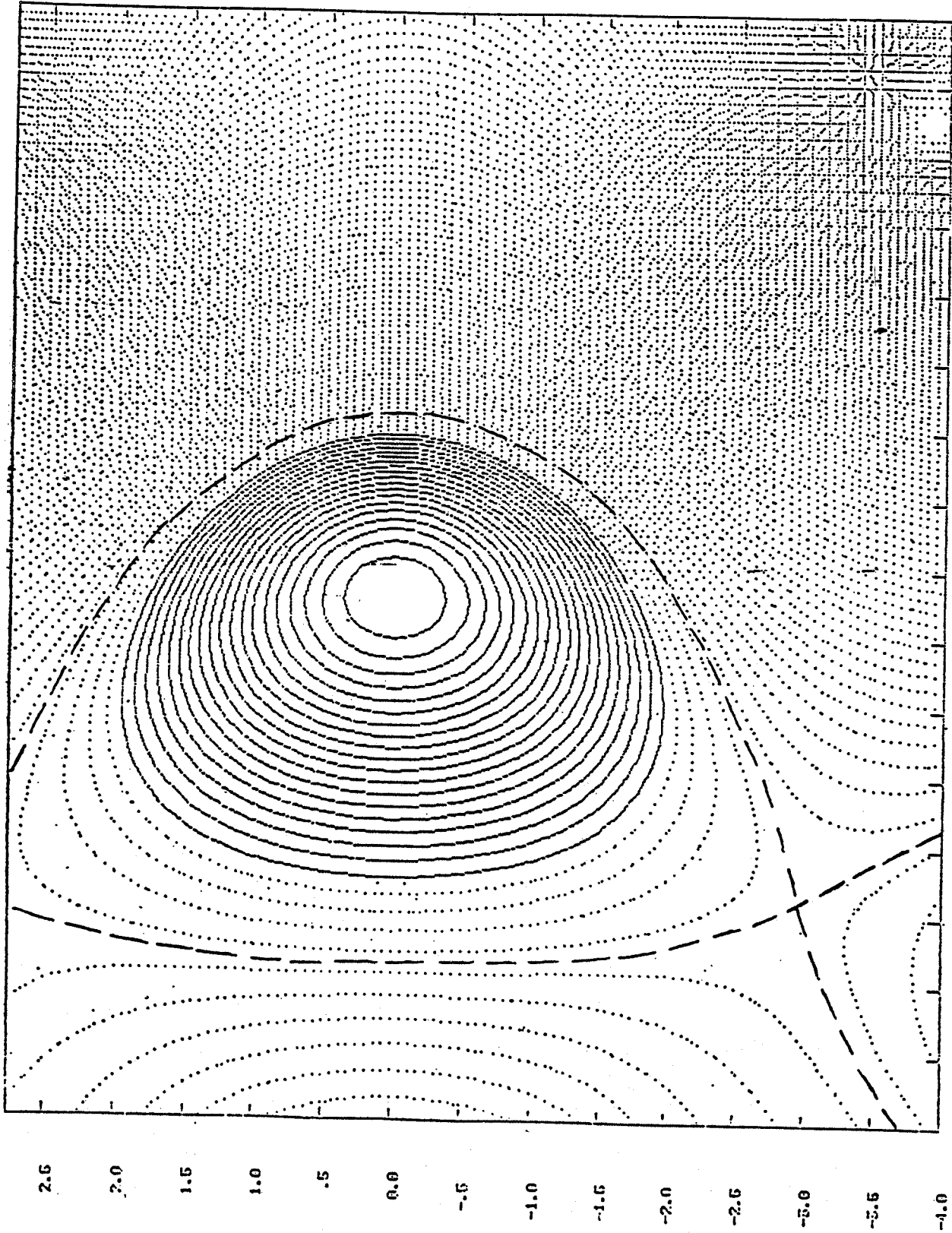
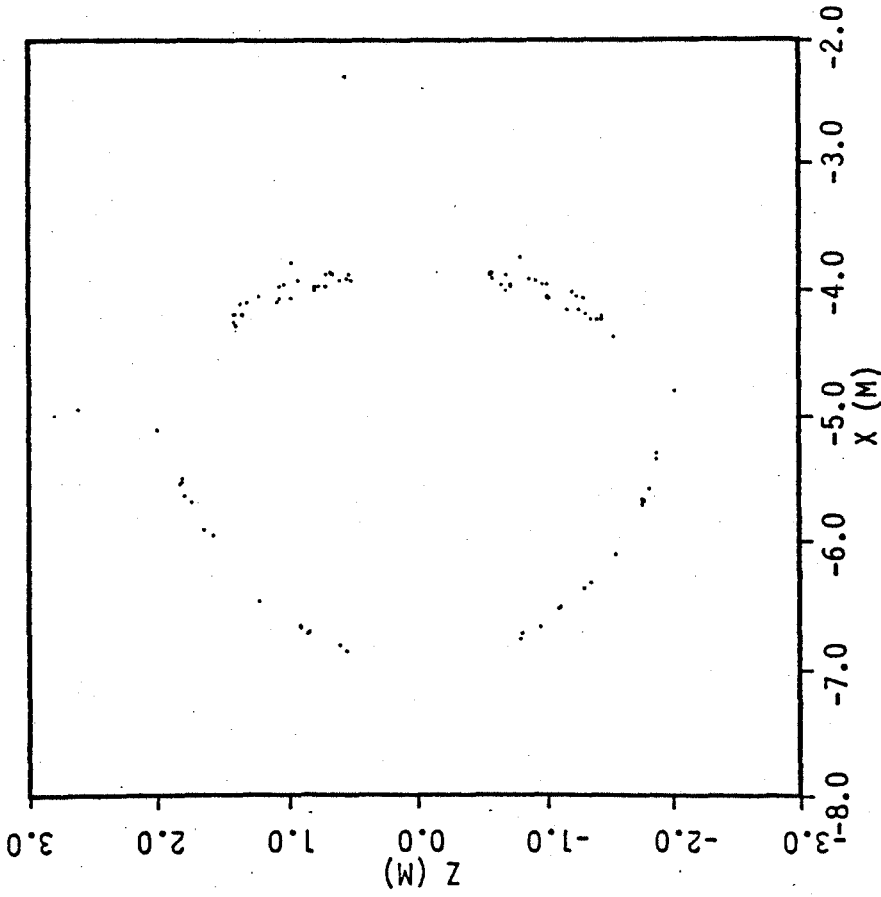


Fig. 10: Axisymmetric MHD equilibrium flux configurations. The space between the plasma boundary and poloidal separatrix is  $> 20$  cm.

FLUX SURFACES



FLUX SURFACES

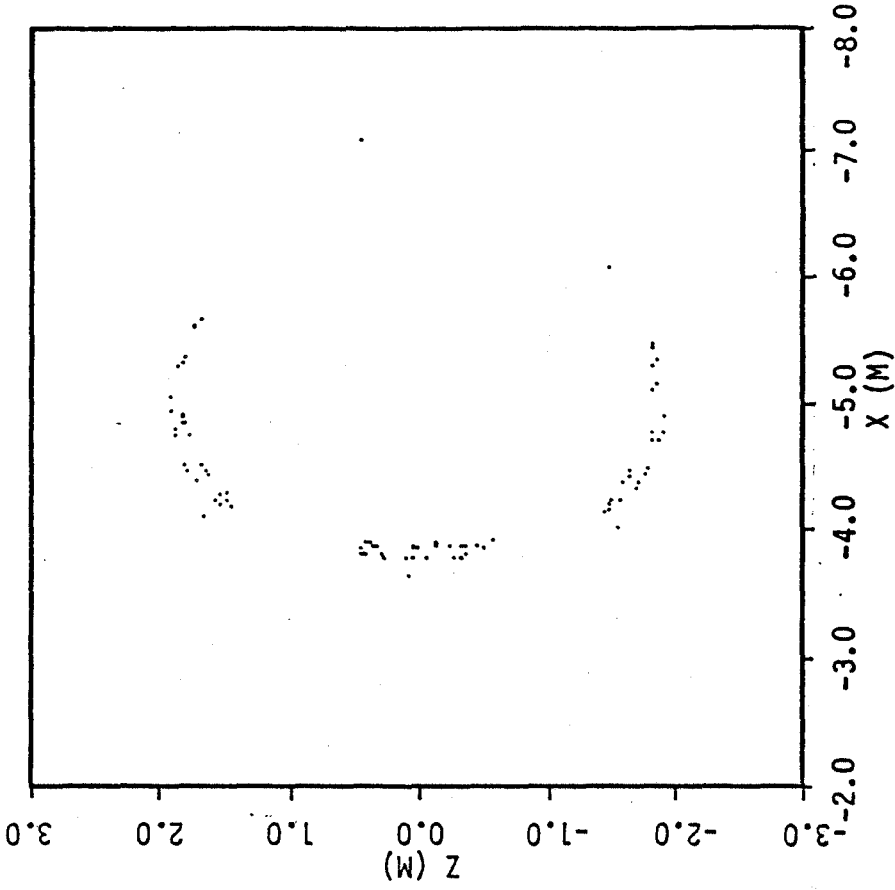


Fig. 11: Flux surfaces at the plasma boundary at  $\phi = 0^\circ, 180^\circ$  for configuration 1. There are island structures, but the points marked by circles begin to wander away and show ergodicity. The field line already leaves the machine through poloidal separatrix at point a. Therefore, it can no longer be followed.



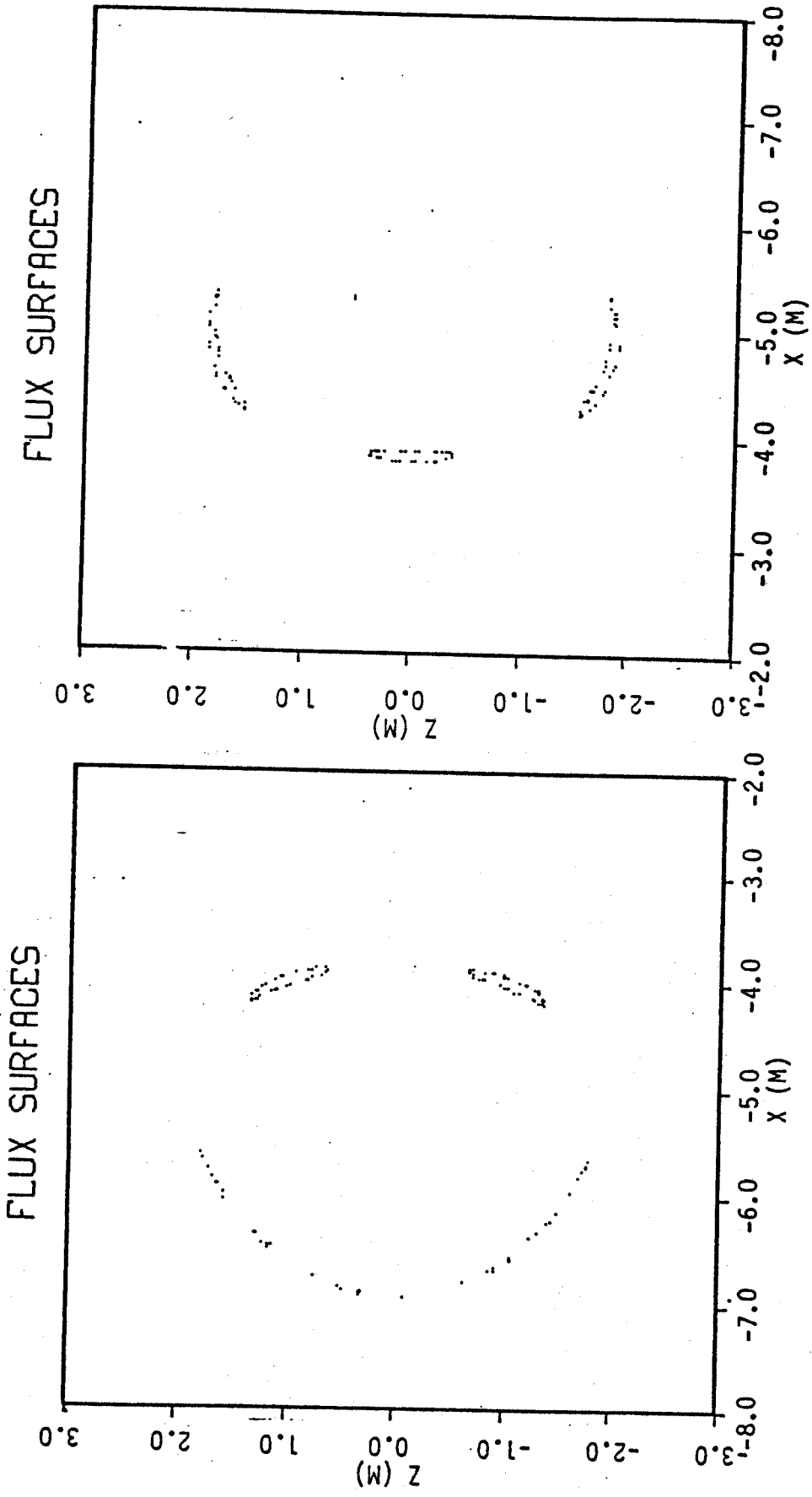
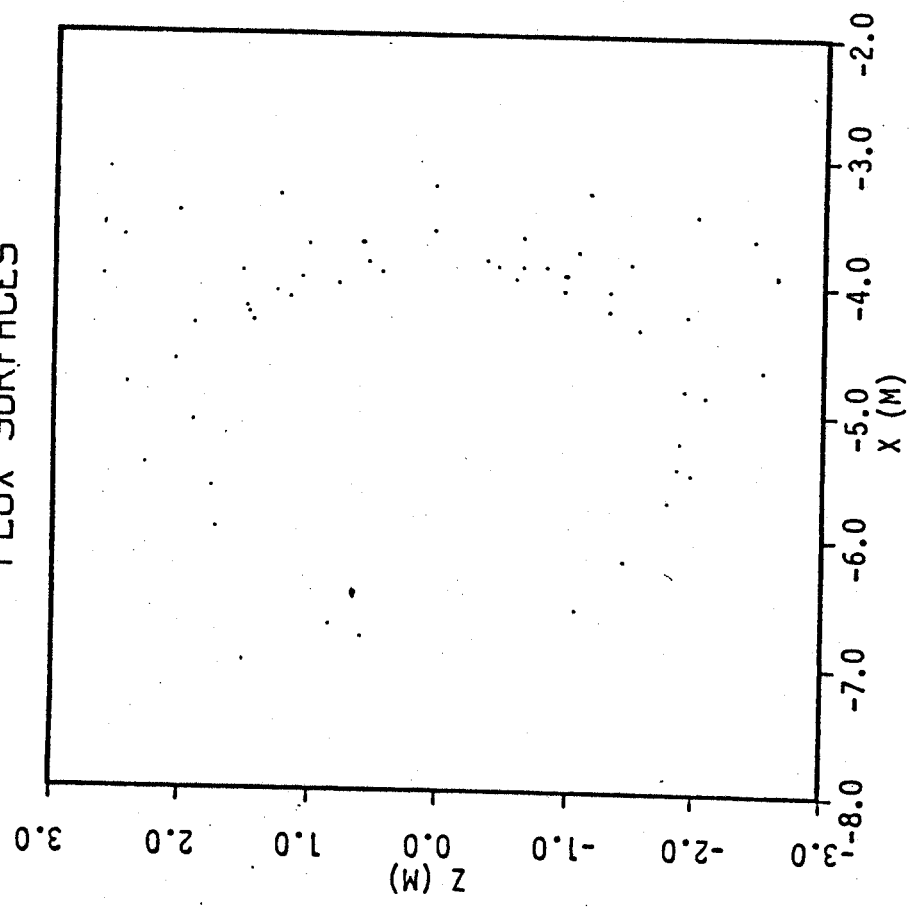


Fig. 12: Magnetic surface at plasma boundary at  $\phi = 0$

FLUX SURFACES



FLUX SURFACES

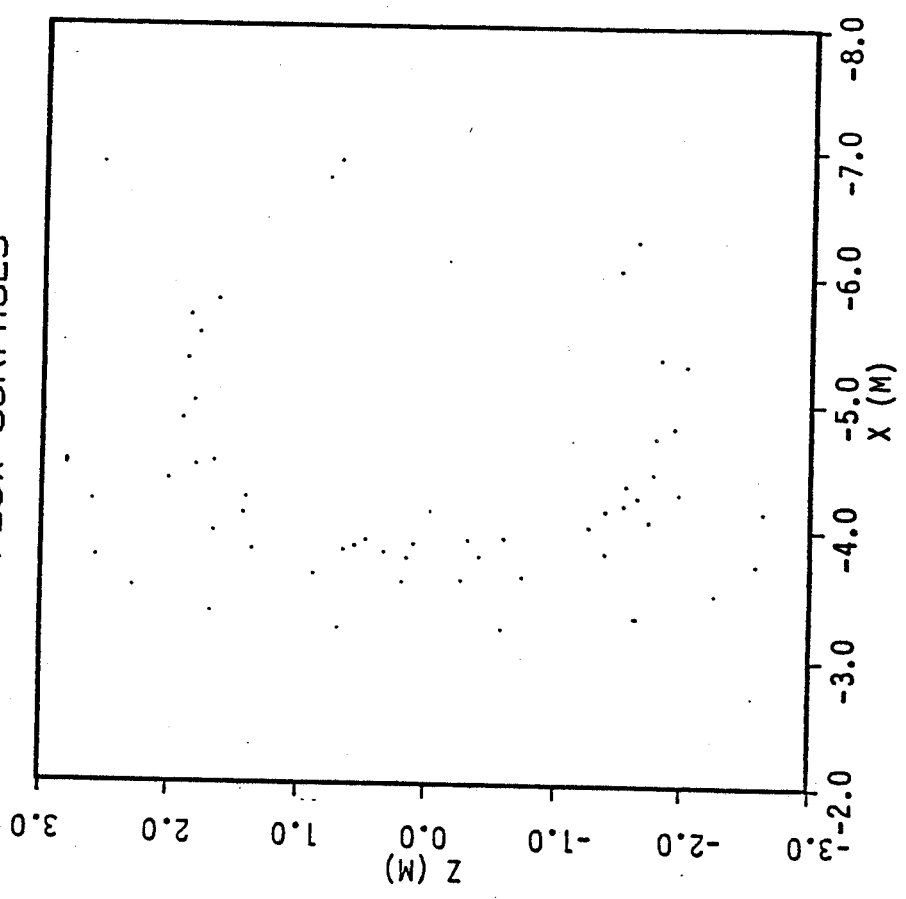
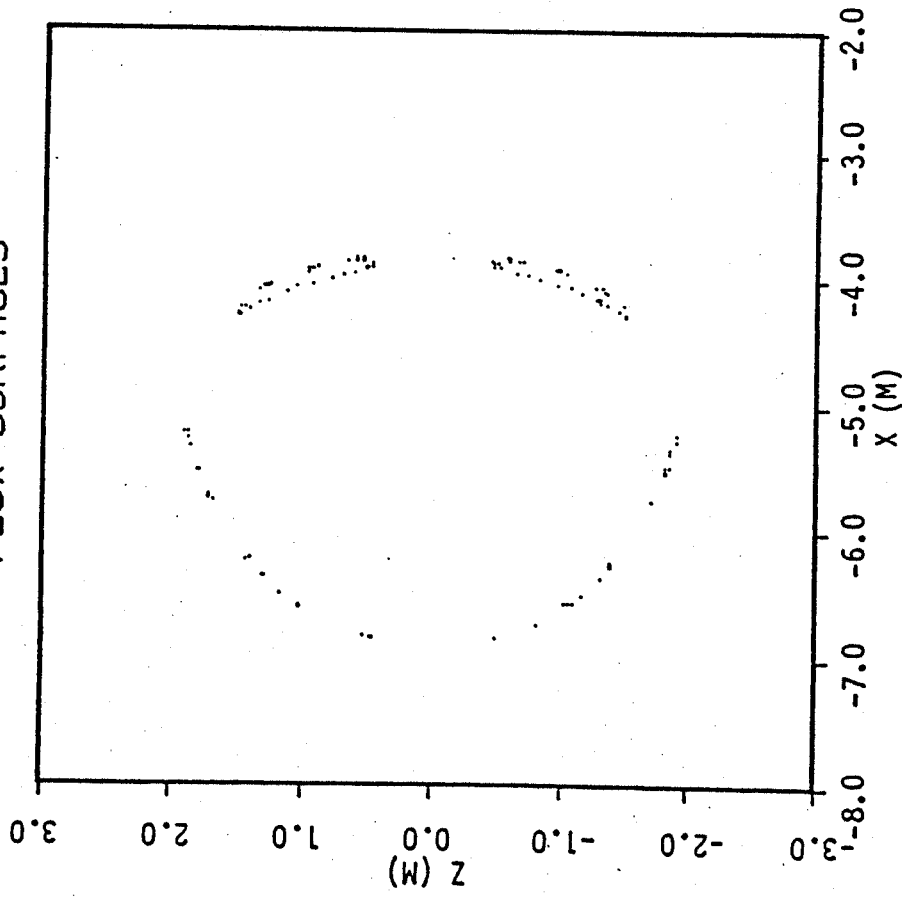


Fig. 13: Flux surfaces at plasma boundary for configuration 5 at  $\phi = 0^\circ$  and  $180^\circ$ .  
The surface is ergodic.

FLUX SURFACES



FLUX SURFACES

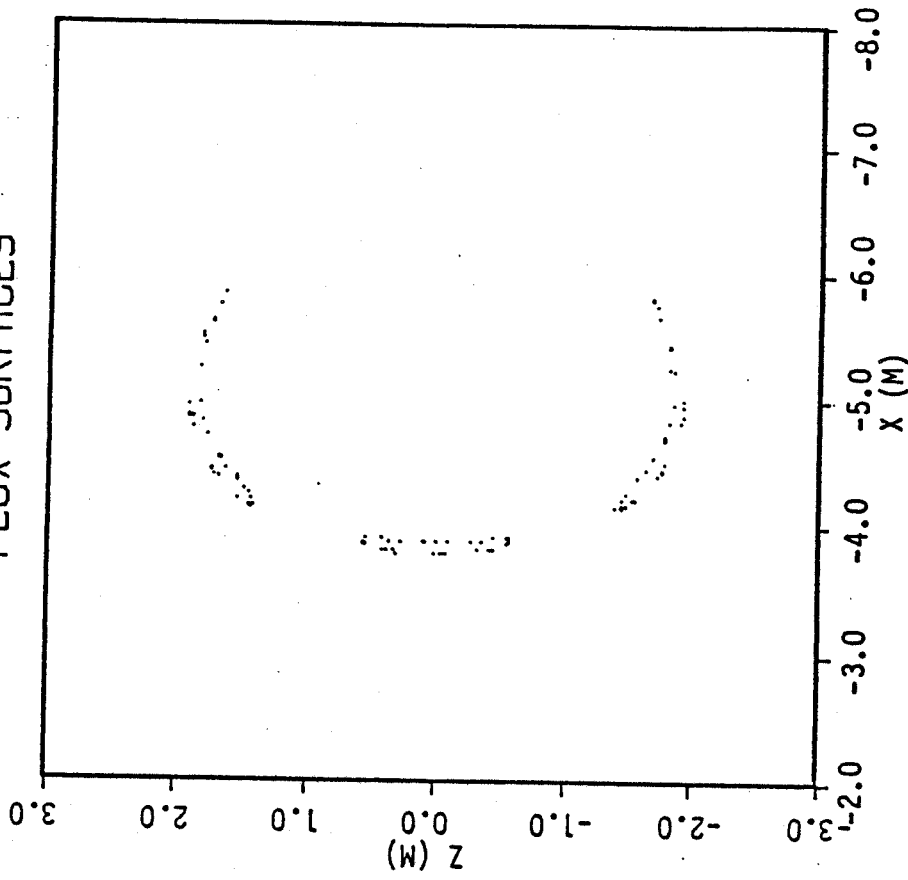
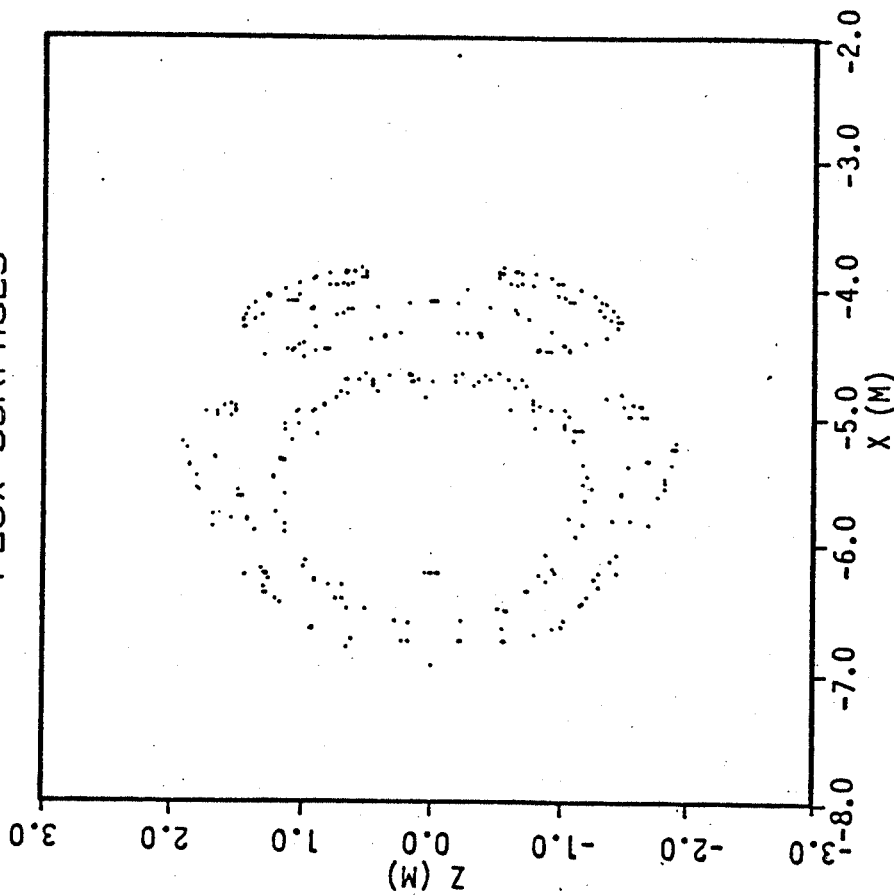


Fig. 14: Flux surface at plasma boundary for configuration 6 at  $\phi = 0^\circ$  and  $180^\circ$ . There are islands, but the surface is nonergodic.

FLUX SURFACES



FLUX SURFACES

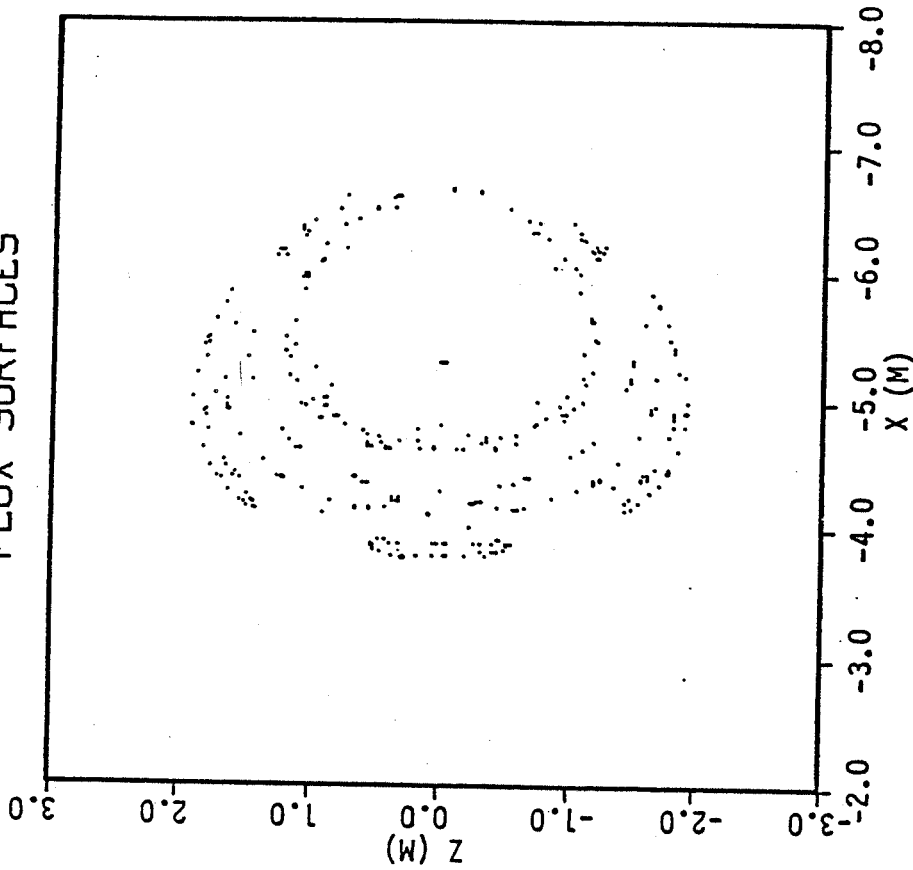
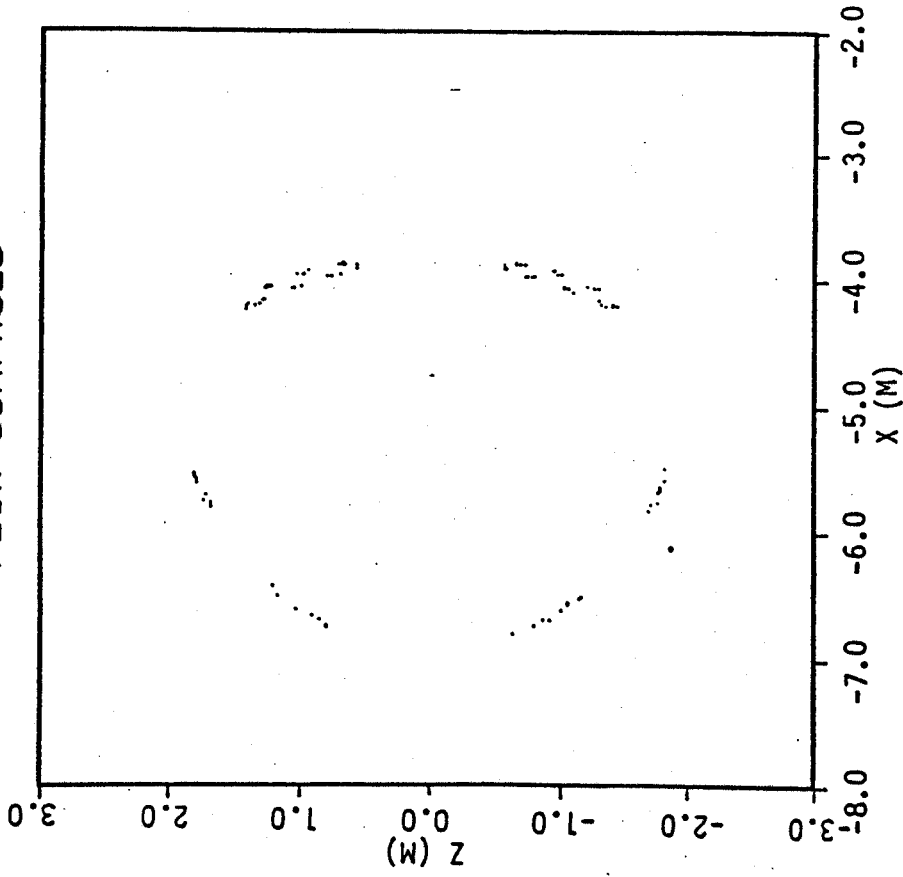


Fig. 15: Four flux surfaces for 3 staged T-coils (cascade bundle divertor). There are islands except at the inner most surface where  $q$  is 1 and no surface is generated.

FLUX SURFACES



FLUX SURFACES

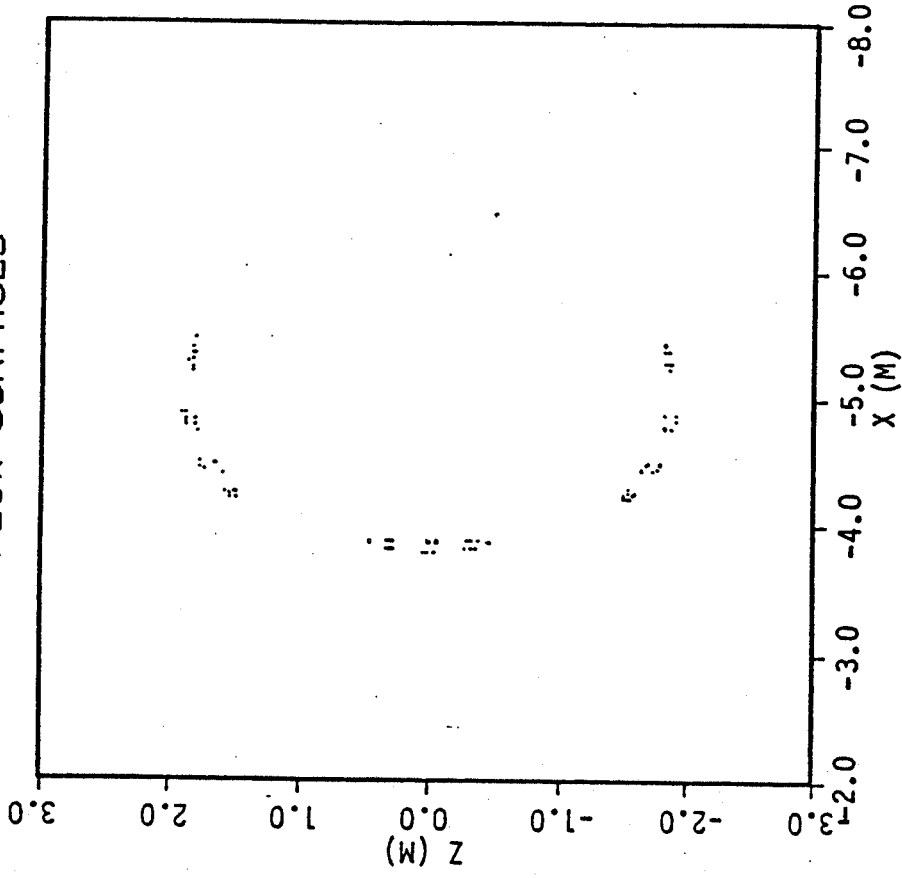


Fig. 16: Flux surface for 4 "T" coils

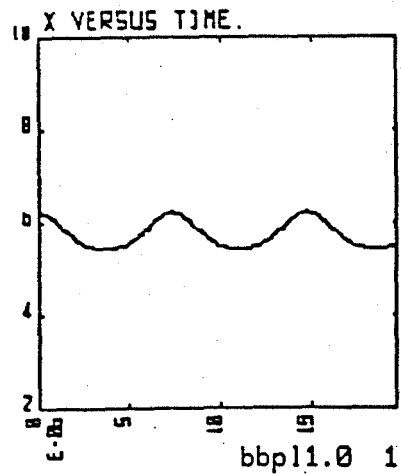
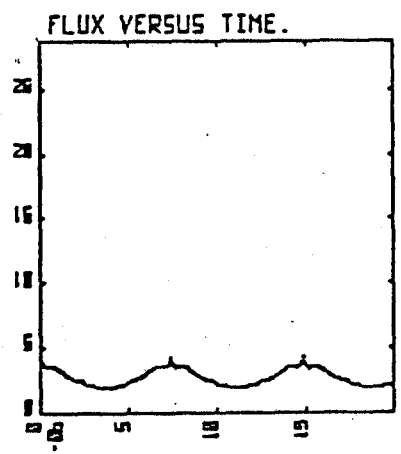
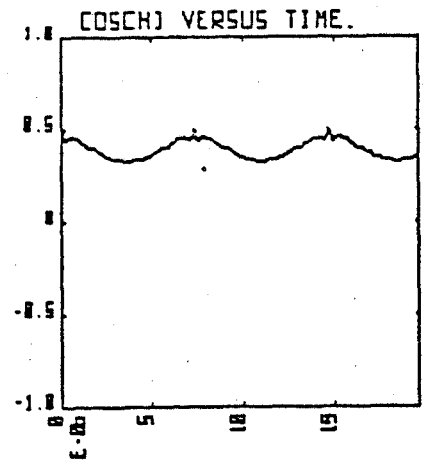
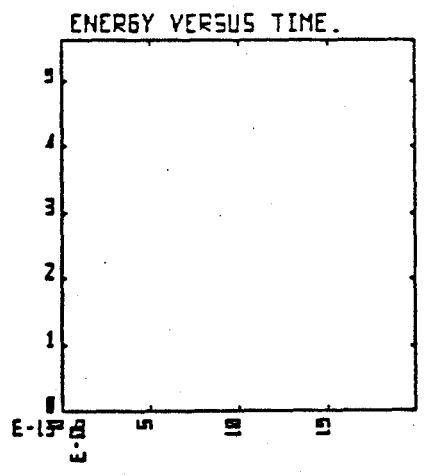
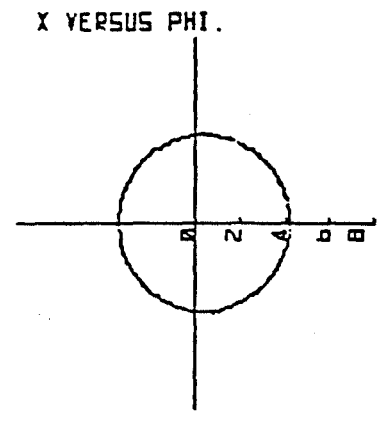
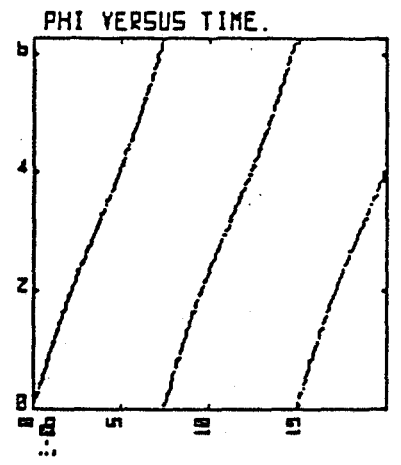
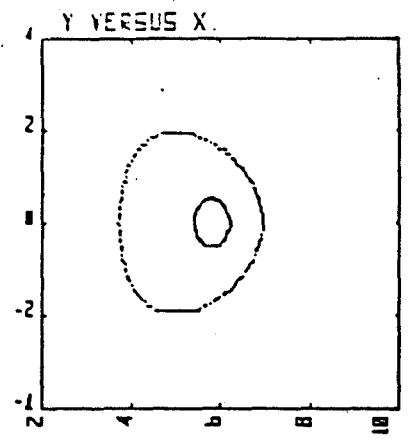
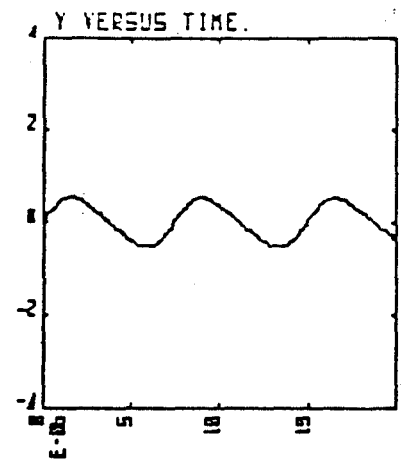


FIGURE 2

bbpl1.0 1 fxalfas3

Fig. 17: Circulating orbit for a 3.5 MeV  $\alpha$ -particle with  $\cos \chi = 0.5$  launched at  $\chi = 6.25$  M. The particle is confined.

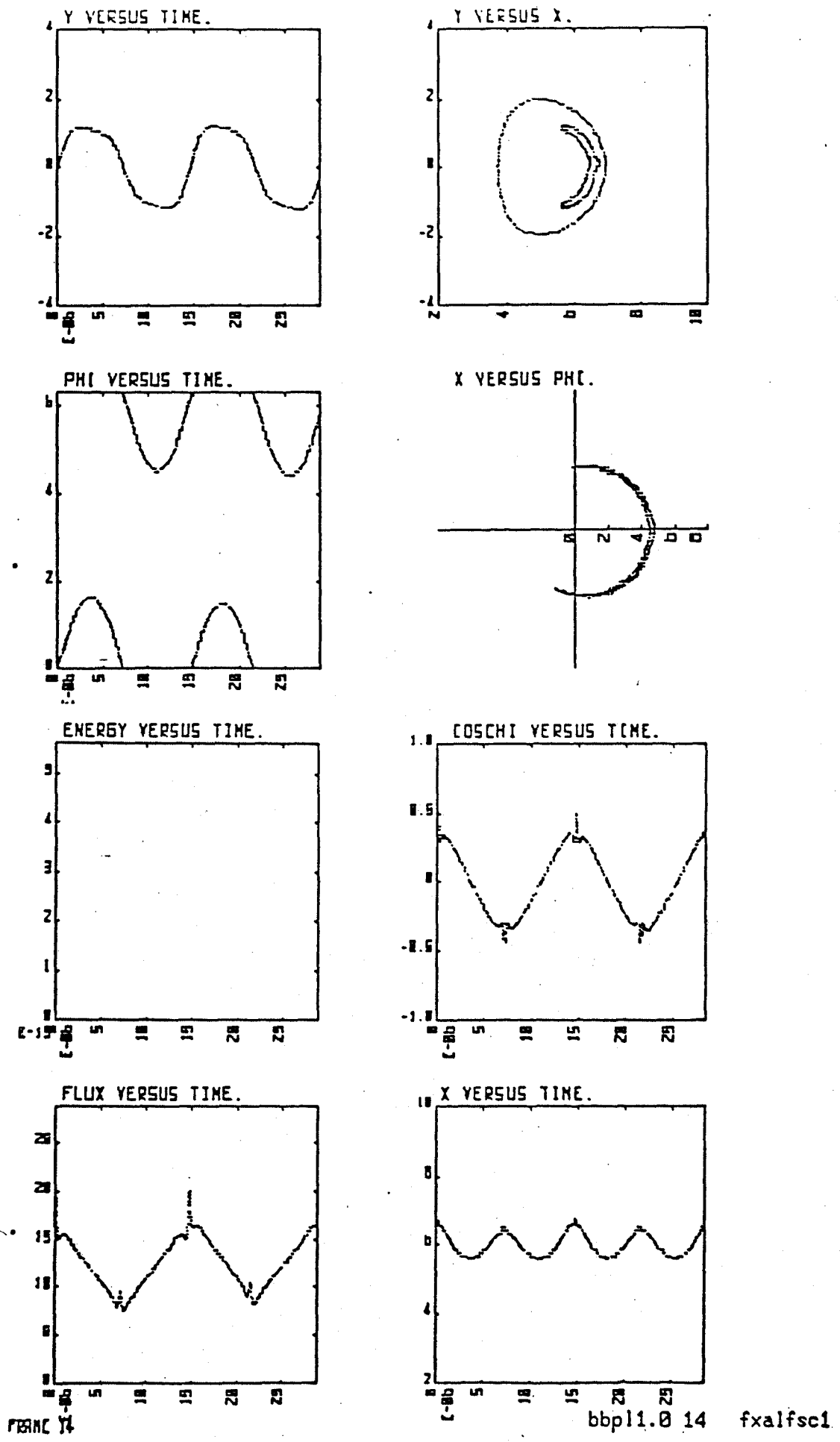


Fig. 18: Banana orbit for a 3.5 MeV  $\alpha$ -particle with  $\cos \chi = 0.5$  launched at  $\chi = 6.5$  M. The particle is confined.

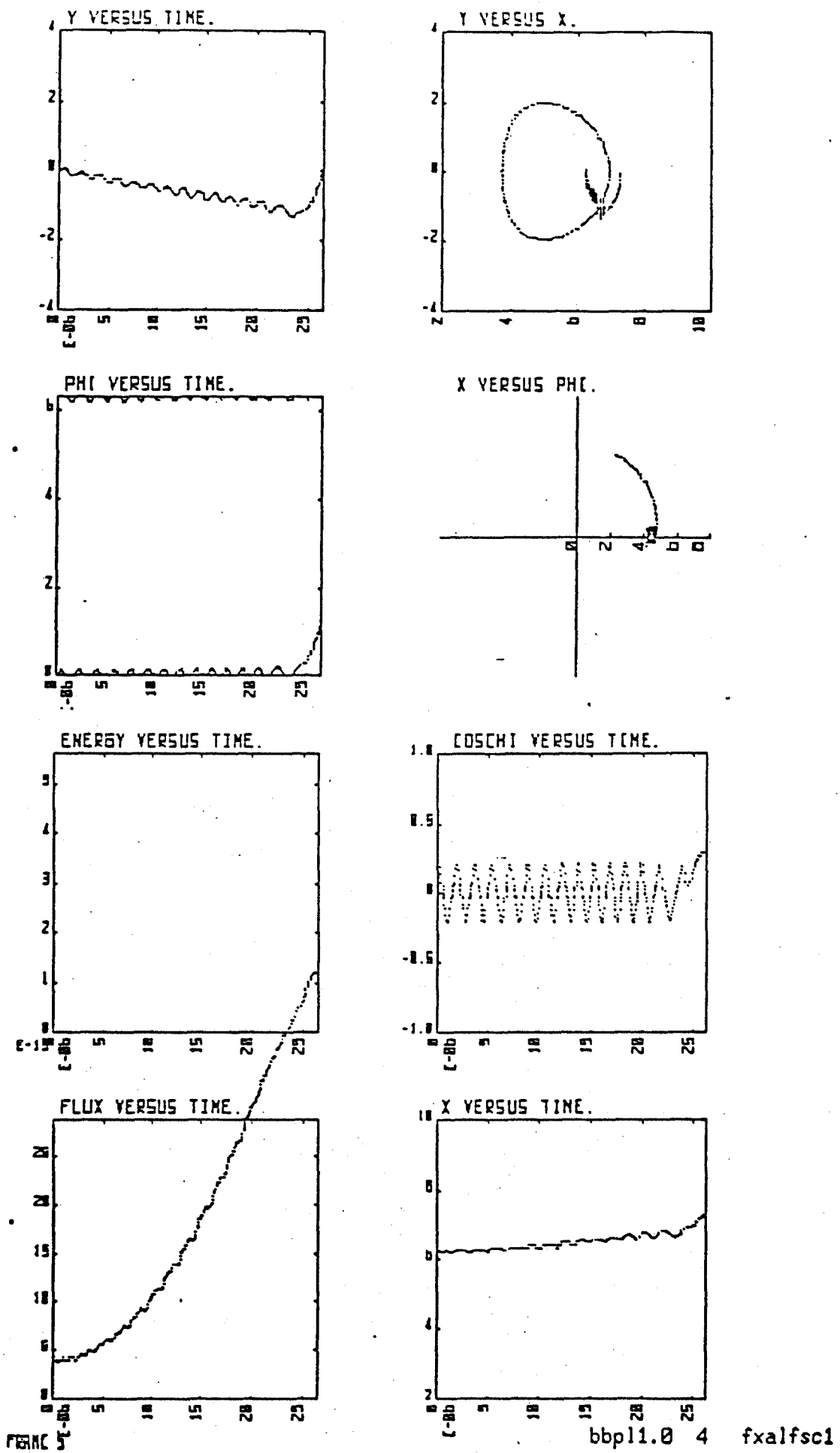


Fig. 19: Ripple trapped orbit for a 3.5 MeV  $\alpha$ -particle with  $\cos \chi = 0.2$  launched at  $\chi = 6.25$  M. The particle is drifting out of plasma.



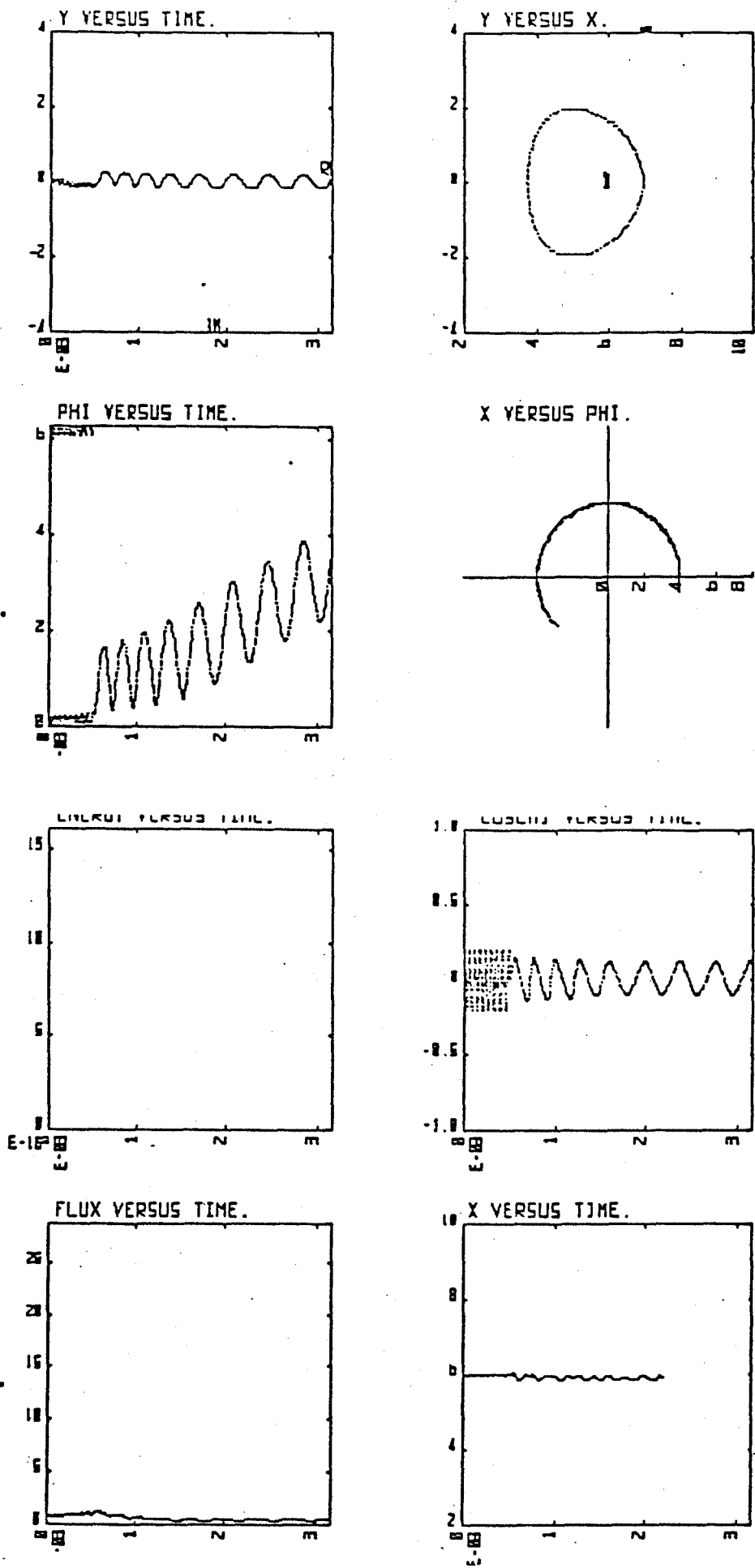
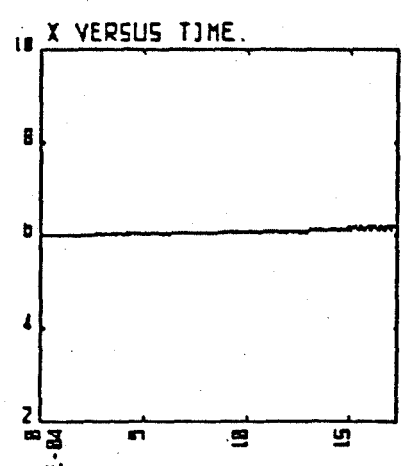
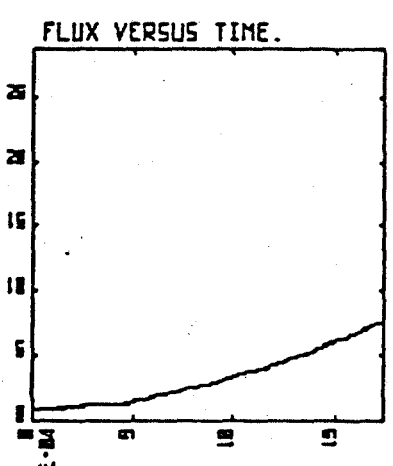
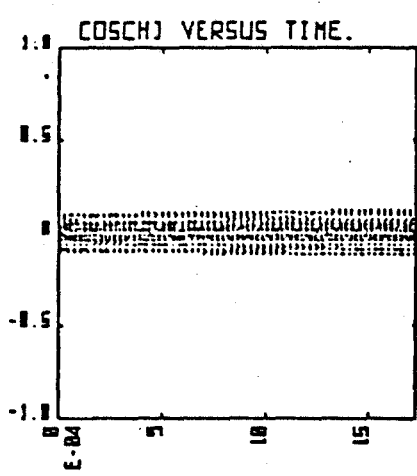
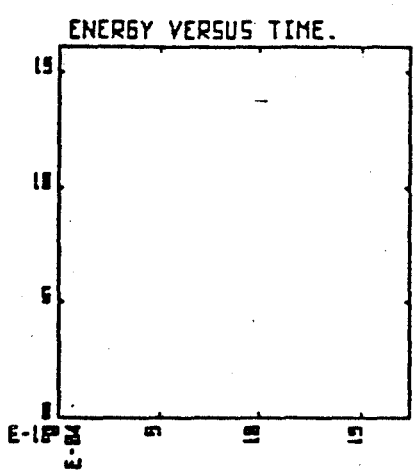
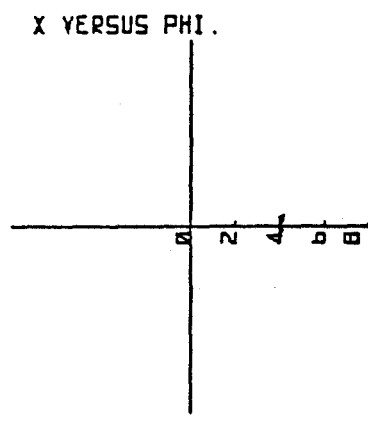
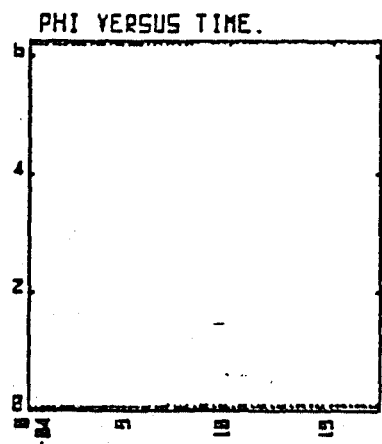
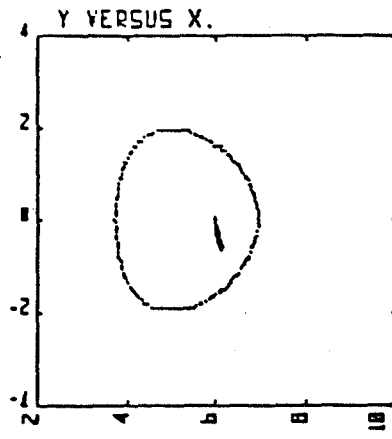
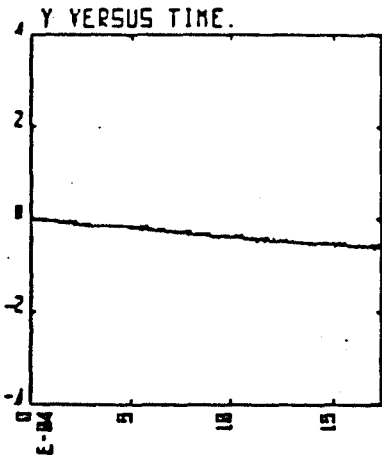


Fig. 20: Trapped thermal particle with 10 keV,  $\cos \chi = 0.2$  launched at 6.0 M. The particle is detrapped when drifting into low ripple region.



78312

Fig. 21: Trapped thermal particle which will be lost.

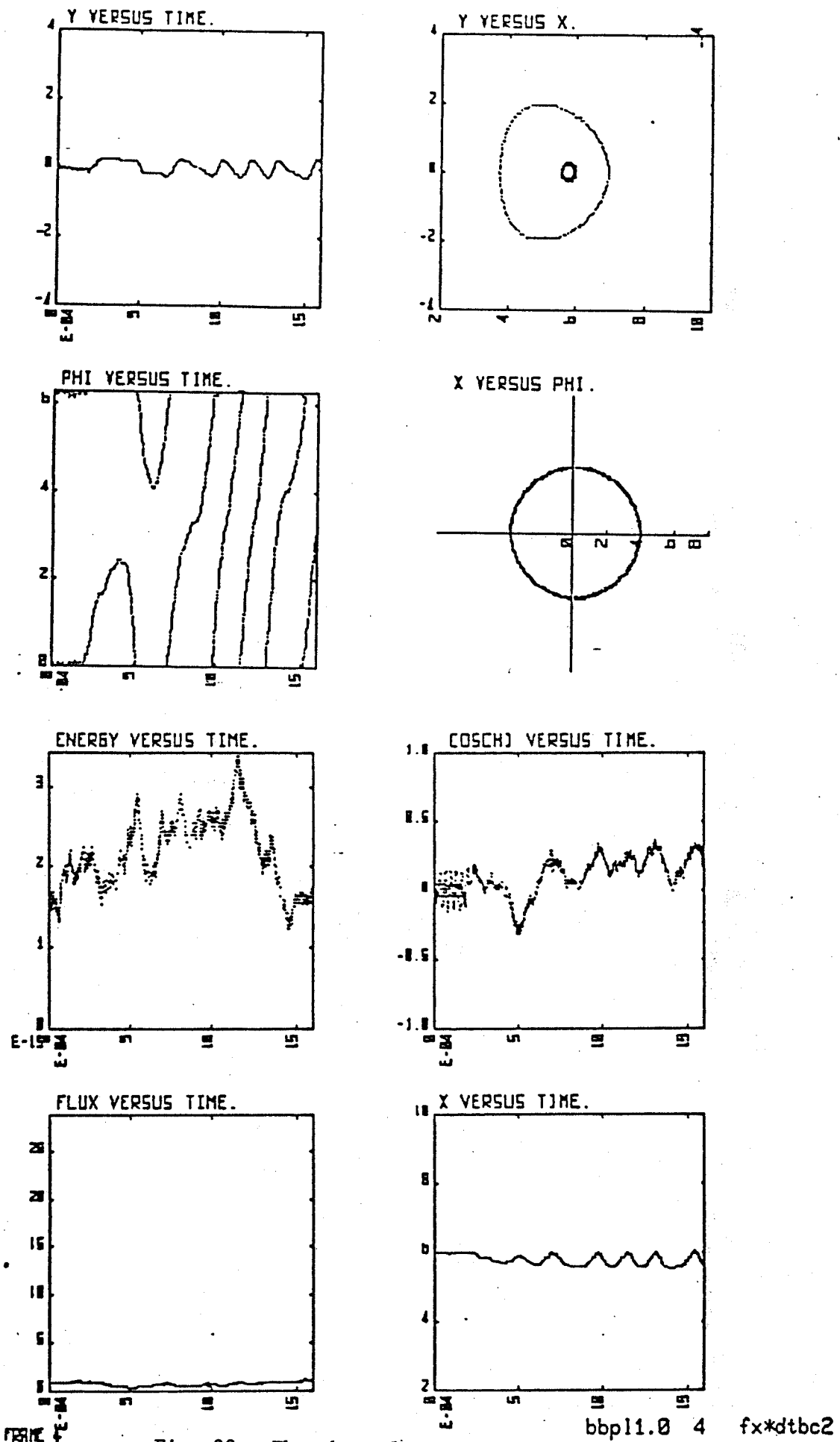


Fig. 22: The thermal particle is detrapped and becomes circulating due to collision.

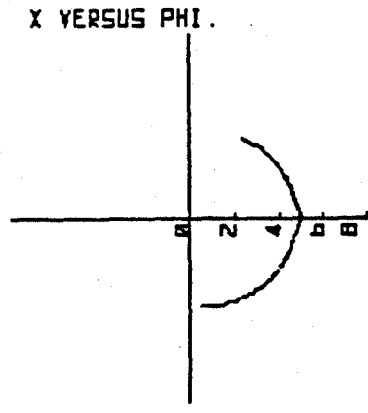
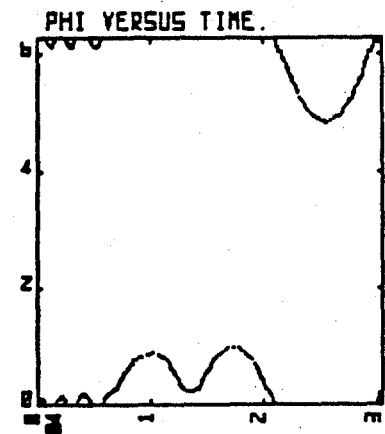
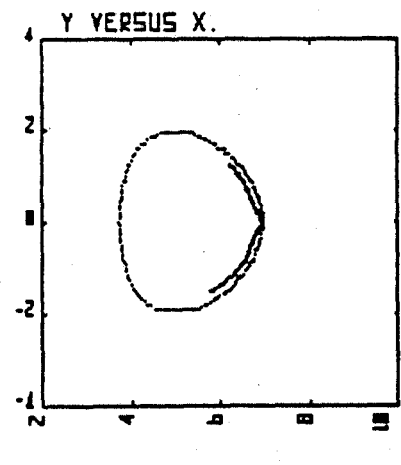
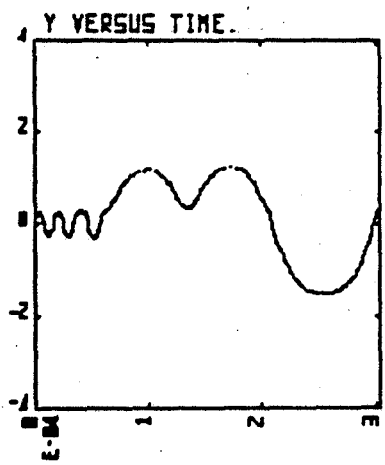
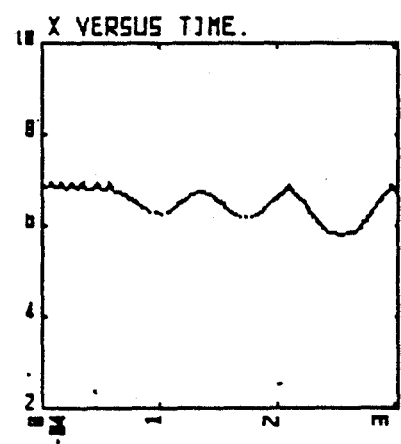
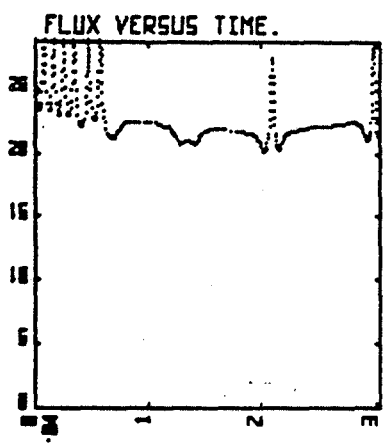
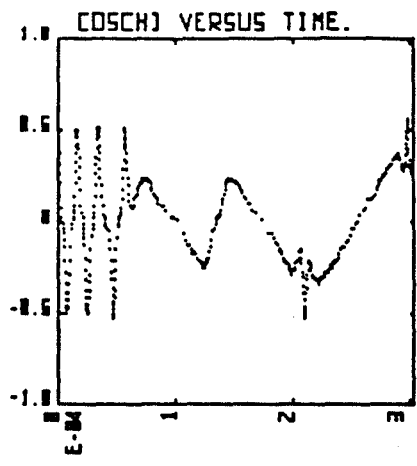
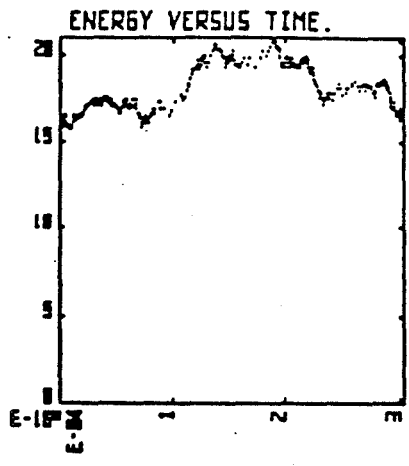
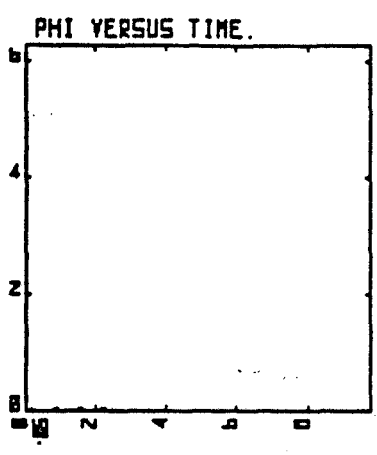
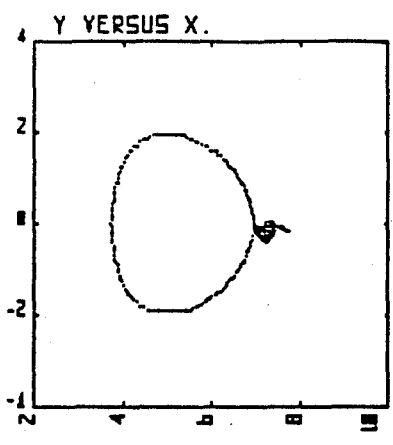
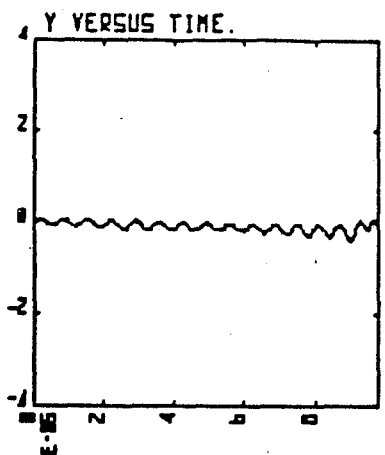


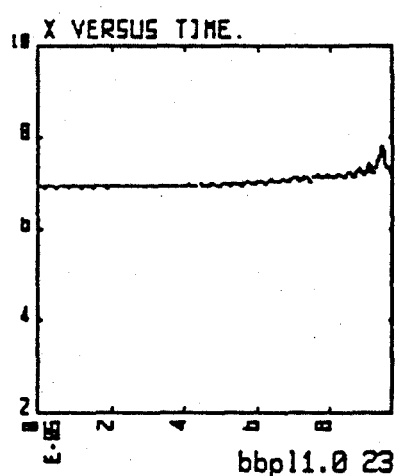
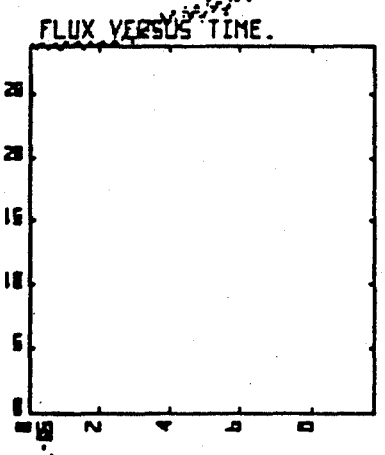
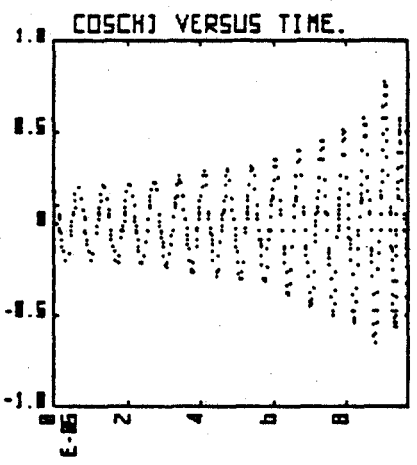
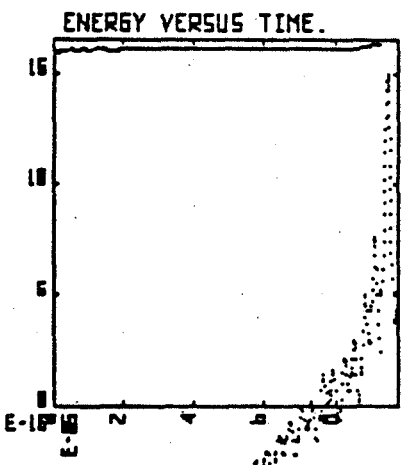
FIGURE 21

Fig. 23: The particle is detrapped and becomes banana orbit due to collision.

bbp11.0 21 fx\*dtaci



X VERSUS PHI.



FRAME 23

bbpl1.0 23 fx\*dtac1

Fig. 24: The particle is drifting into divertor throat.

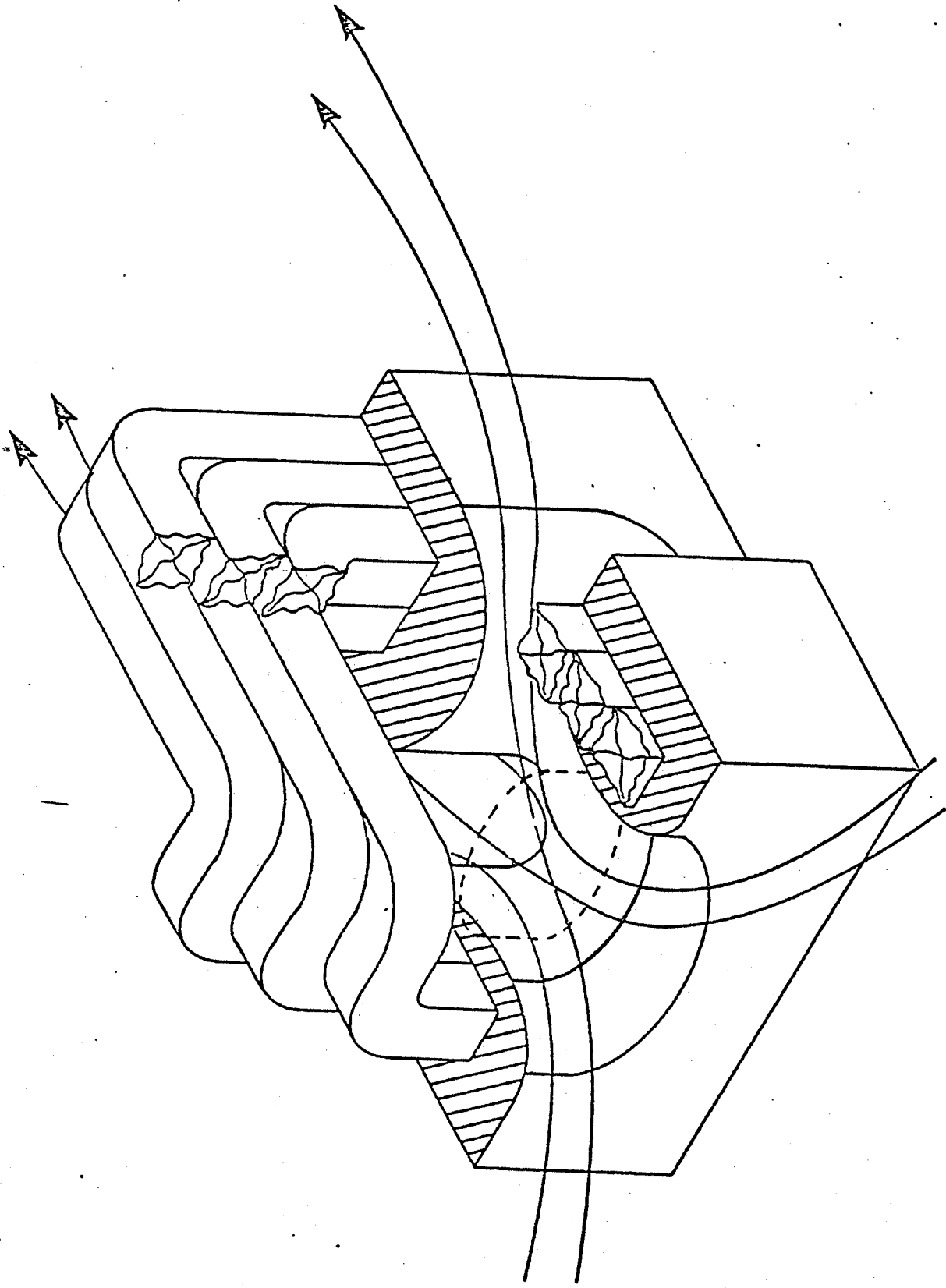


Fig. 25: Trimetric view of an advanced bundle divertor configuration with structure.

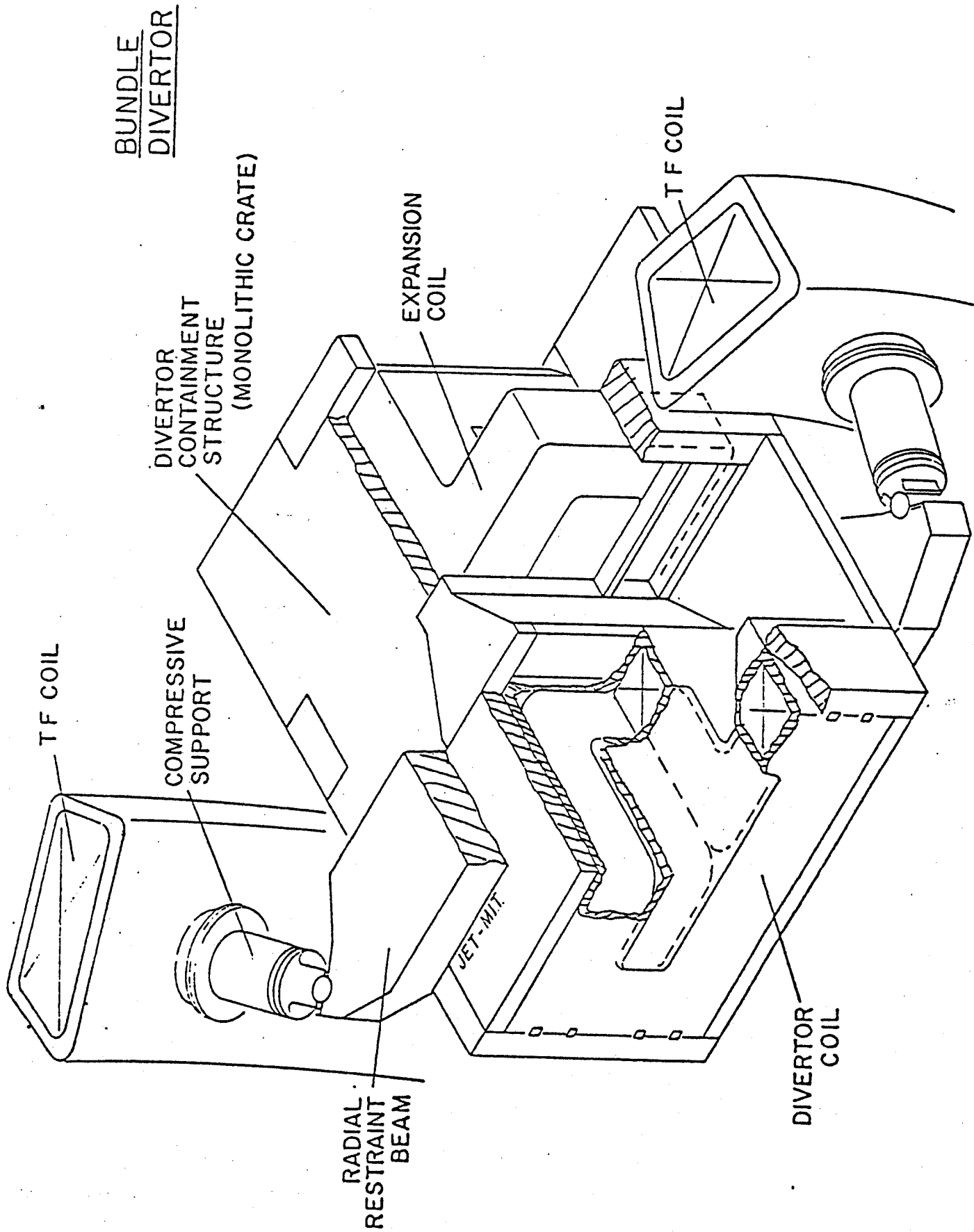
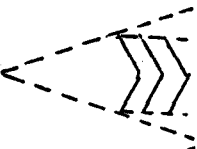
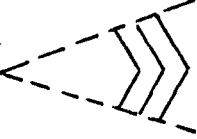
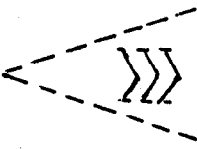
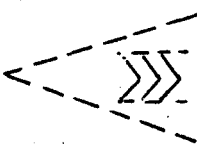
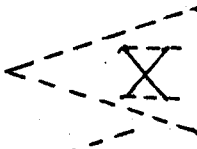
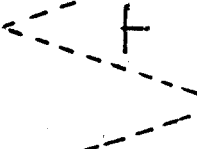
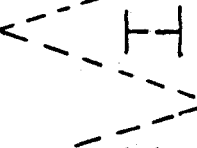
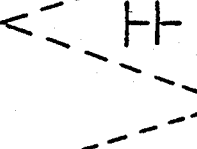
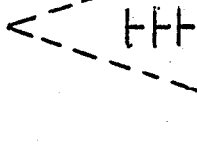


Fig. 26: Engineering concept of the bundle divertor/assembly.

TABLE 1

Comparison of bundle divertor configurations and characteristic parameters. The major radius of the separatrix is  $R_{sep} = 7.0$  m. The distance between the separatrix and conductor is 1.0 m.  $J_D$  The coil cross-section is 50 cm X 50 cm.

	Large Divertor	$I_D$ (MA-T)	$J_D$ $\frac{kA}{cm^2}$	Flux Surface Property
1.	 Solenoid	9.32, 4.66, 4.66	3.7	Not Traced
2.	 Conical Section	8.65, 4.32, 4.32	3.5	Nonergodic islands
<u>Small Divertor</u>				
3.	 Solenoid	17.5, 8.75, 8.75	7.0	Ergodic islands
4.	 Rectangular	13.4, 6.7, 6.7	5.4	Nonergodic
5.	 Circular X-type	13.35, 13.35	5.3	Not Traced
6.	 T-shape	9.84	3.9	Ergodic
7.	 Reverse T	7.9, 7.9	3.2	Not Traced
8.	 Double T	8.3	3.3	Nonergodic islands
9.	 Cascade T	8.75	3.5	Nonergodic islands